Journal of Materials Chemistry B

ROYAL SOCIETY OF CHEMISTRY

PAPER

View Article Online
View Journal | View Issue

Cite this: J. Mater. Chem. B, 2025, 13, 288

Near-IR nanolignin sensitizers based on pyrene-conjugated chlorin and bacteriochlorin for ROS generation, DNA intercalation and bioimaging†

Kunal Gogde,[ab] Seema Kirar,[a] Anil Kumar Pujari,[ac] Devesh Mohne,[ac] Ashok Kumar Yadav[b] and Jayeeta Bhaumik *[a]

Near-infrared (NIR) fluorescent agents are extensively used for biomedical imaging due to their ability for deep tissue penetration. Tetrapyrrole-based photosensitizers are promising candidates in this regard. Further, the extended conjugation of such macromolecules with chromophores can enhance their fluorescence efficiency and DNA intercalation ability. Herein, pyrene-conjugated NIR photosensitizers, such as chlorin (PyChl) and bacteriochlorin (PyBac), were synthesized from the corresponding pyrene–porphyrin (PyP). The correlation between the theoretical and experimental optical properties (absorption and fluorescence spectroscopy results) was determined using the DFT/TD-DFT computational approach. Next, studies on the photophysical properties, reactive oxygen species (ROS) production, and DNA binding were conducted on these macrocycles to study the effect of pyrene conjugation on the pyrrolic ring. Furthermore, each photosensitizer was loaded into lignin nanoparticles (LNPs) using the solvent–antisolvent method to accomplish fluorescence-guided imaging. The developed near-IR chlorin- and bacteriochlorin-doped lignin nanocarriers (PyChl-LNCs and PyBac-LNCs) exhibited significant *in vitro* singlet oxygen generation upon red LED light exposure. Moreover, these macrocycle-loaded nanolignin sensitizers showed good fluorescence-guided bioimaging with fungal cells (*Candida albicans*). Further, the nanoprobes exhibited pH-dependent release profiles for biological applications. These nanolignin sensitizers demonstrated promising potential to be utilized in near-IR image-guided photodynamic therapy.

Received 24th July 2024,
Accepted 18th October 2024

DOI: 10.1039/d4tb01627k

rsc.li/materials-b

Introduction

Near-infrared-assisted photodynamic therapy (PDT) and bioimaging are effective treatments for eradicating microbes.[1] Near-IR photosensitizers could be useful owing to their unique optical properties that utilize the phototherapeutic window (*i.e.* 650–850 nm).[1,2] Since the last decade, near-IR (NIR) fluorophores have attracted much attention for the non-invasive imaging of microbial cells.[1] Among natural mimics, bacteriochlorins, which are present in bacteriochlorophylls, are attracting interest as bacteriochlorophyll-based pigments can harvest far-red to near-infrared light.[3,4] Chemically, they feature the 18-π-electron conjugation inside the porphyrin ring connected by four methylene bridges and two reduced pyrroles on the opposite sides.[5] Bacteriochlorin structure does not require two peripheral double bonds to maintain aromaticity.[3,5] Thus, reducing one or both bonds of porphyrin leads to chlorin and bacteriochlorin, respectively. They have unique optical properties that make them suitable for absorption in the phototherapeutic window.[5,6] These near-IR light-absorbing photodynamic agents can penetrate deep tissue during PDT.[4–6] Various π-electron chromophores are being utilized to develop novel probes with unique photophysical characteristics, such as a high quantum yield and longer fluorescence lifetime.[7] For example, the substitution of aromatic chromone, naphthalene, pyrene, and pyrazole can be used for the study.[7] Among these, pyrene is a versatile, well-studied, and highly fluorescent polycyclic aromatic ring, and its attachment to near-IR photosensitizer can provide intramolecular charge transfer, which could enhance optical properties.[8] Thus, pyrene attachment can make better analytical and diagnostic probes for bioimaging and therapy. The pyrene ring could also help to bind with DNA. Further, it can assist in microbial and

[a] Center of Innovative and Applied Bioprocessing (CIAB), Department of Biotechnology (DBT), Government of India, Sector 81 (Knowledge City), S. A. S. Nagar 140306, Punjab, India. E-mail: jayeeta@ciab.res.in, jbhaumi@gmail.com
[b] University Institute of Pharmaceutical Sciences, Panjab University, Sector 14, Chandigarh 160306, India
[c] Indian Institute of Sciences Education and Research (IISER), Sector 81 (Knowledge City), S. A. S. Nagar 140306, Punjab, India

† Electronic supplementary information (ESI) available Instruments and methods, materials ad chemicals, tables. See DOI: https://doi.org/10.1039/d4tb01627k

cancerous DNA intercalation during photodynamic therapy.[9,10] Hence, we designed pyrene-conjugated near-IR photosensitizers that could serve as unique pharmacophores for near-IR imaging.

Bacteriochlorin-based NIR photosensitizers have been reported for photodynamic and bioimaging applications in the past two decades. Being second-generation, they are considered promising agents for photodynamic therapy and bioimaging compared to natural bacteriochlorophyll.[2,9] Recent examples are platinated bacteriochlorins, tetrafluorophenyl bacteriochlorin, cationic bacteriochlorins, and 5,10,15,20-tetrakis[4-(3-*N*,*N*-dimethylaminopropoxy)phenyl] chlorin for PDT and bioimaging applications.[2,11–14] However, they have a few drawbacks, such as a lower aqueous solubility, self-aggregation, and lack of targeting, which limit the utilization of porphyrin, chlorin, and bacteriochlorin for biological applications.[14] A nanotechnological approach can be utilized to deliver the photosensitizer using a drug-delivery system to improve these properties.[15–17] Diverse ranges of nano-photosensitizers, such as metal nanoclusters, carbon dots, colloidal metal photosensitizers based on a silica shell, and gold nanocarriers have been reported for NIR bioimaging and ROS-enhanced photodynamic therapy.[18] One such example is NIR-absorbing platinum(II)–acetylide conjugated polymers (CPs) containing BODIPY, which exhibited potential as phototheranostic agents in cancer treatment.[19]

Agri-biomass-derived lignin, a non-toxic, biodegradable polymer, has been preferred to prepare nanoparticles that can enhance the efficacy and targeted delivery of hydrophobic photosensitizers.[20–22] The aromatic structure of lignin can be beneficial in phototheranostic applications due to the presence of phenyl propane units, such as sinapyl, coniferyl, and *p*-coumaric alcoholic hydroxyl, and carboxyl groups on the surface of lignin.[23–26] It provides unique photoluminescent properties, with utility in photodynamics and bioimaging, and some studies have shown lignin's biocompatibility with cells.[27,28] Thus, lignin nanoparticles could be a promising platform for the delivery of NIR photosensitizers. The highly polyphenolic chemical structure of lignin provides the probability of non-covalent interactions, such as π–π stacking and H-bonding, with the hydrophobic photosensitizer(s).[20–22] Conclusively, these properties enhance the loading efficiency of photosensitizer drugs.[26,29] The biocompatibility of lignin nanoparticles has been tested in both *in vitro* cell viability studies as well as in *in vivo* studies.[26] These studies revealed that they formed non-toxic byproducts.[26] Also, lignin is the most abundant biopolymer after cellulose, and its ease of availability makes it widely accessible.[23,24]

In this study, pyrene-conjugated near-IR photosensitizers with chlorin and bacteriochlorin were synthesized using porphyrin. Furthermore, they were characterized by various spectroscopic techniques. An *in silico* TD-DFT study was conducted to correlate the theoretical study with the optical properties, and it also provided the molecular orbital electron-density distributions and energies. Due to the lack of water solubility and self-aggregation, their use in *in vitro* and *in vivo* biological studies has been limited to date.[12,20] Hence, we loaded photodynamic agents (PyP, PyChl, and PyBac) in the lignin nanoparticles. Analysis of singlet oxygen generation and ROS production by the photosensitizers (PyP, PyChl, and PyBac) and their nanoformulations was performed using a green/red-light-emitting diode (LED) light (12 W). The NIR fluorescence bioimaging potential of the nanoformulations was validated using *Candida albicans* fungal cells. The photosensitizers (**8**, **9a**, and **9b**) with a fluorophore group, *i.e.* pyrene, displayed a higher DNA binding affinity and enhanced fluorescence properties.

Results and discussion

Synthesis and characterization of pyrene-conjugated near-IR photosensitizers

The hydrogenation or reduction of porphyrins is one of the common approaches to scaling up bacteriochlorin.[5,30,31] Whitlock *et al.* reported the first diimide reduction of porphyrin under mild conditions.[31] To reduce the long reaction process, Nascimento *et al.* modified and optimized the diimide reduction of porphyrin under microwave irradiation and managed to scale up the bacteriochlorins with higher yields (65% and 85%).[30] Here, pyrene–porphyrin was synthesized by modifying previously reported methods.[22,32–36] The starting aldehyde (benzaldehyde or 2-pyrene carboxaldehyde) and pyrrole were reacted under solvent-free conditions in the presence of indium chloride to obtain *meso*-substituted dipyrromethanes (DPMs) [Scheme 1(A)].[32] Pyrene-dipyrromethane (**3**) was

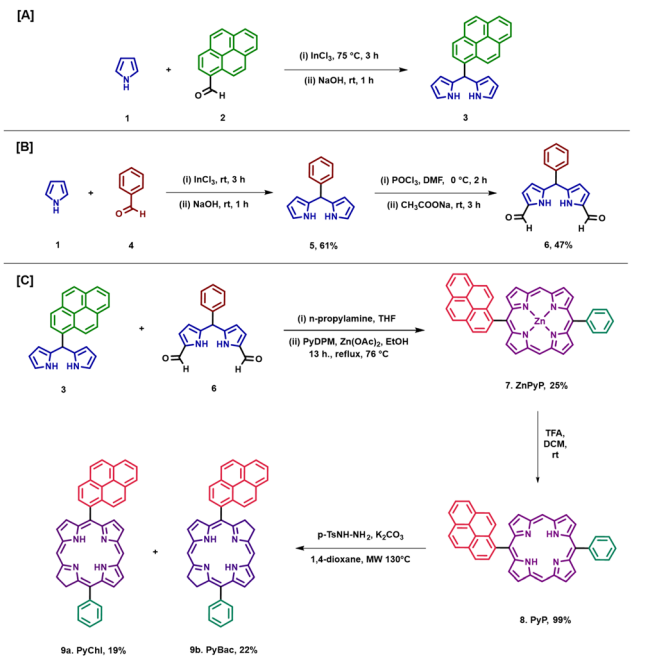

Scheme 1 (A) Synthesis of pyrene–dipyrromethane. (B) Synthesis of phenyl dipyrromethane and 1,9-diformyl dipyrromethane. (C) Synthesis of 5-[4-pyrene]-15-(4-phenyl) bacteriochlorin, and 5-[4-pyrene]-15-(4-phenyl) chlorin.

characterized by ^{1}H and ^{13}C-NMR and mass spectroscopy (Fig. S2, S3, and S7 ESI†). Furthermore, diformylated phenyl dipyrromethane was synthesized by adding the Vilsmeier reagent (a mixture of $POCl_3$ in DMF solvent) to phenyl dipyrromethane (**5**) [Scheme 1(B)]. Phenyl dipyrromethane (**5**) and diformyl phenyl dipyrromethane (**6**) were characterized as per our previous work.[36] Zn-metallated porphyrin (ZnPyP; **7**) was synthesized by the condensation of pyrene DPM (**3**) and diformylated DPM (**6**) in ethanol *via* a McDonald-type reaction, and the yield obtained was up to 25%.[32] Zn(II) pyrene–porphyrin (**7**) was characterized by mass spectroscopy and UV-vis spectroscopy (Fig. S8 and S16 (i), ESI† respectively). With this ZnPyP (**7**), the demetallation reaction was performed to obtain free-base pyrene–porphyrin, PyP (**8**) in a 99% yield [Scheme 1 (C)]. The pyrene–porphyrin (**8**) was confirmed by UV–vis, fluorescence spectroscopy, ^{1}H NMR, and mass spectroscopy [Fig. 1 (i), (ii) and ESI,† Fig. S4, S9]. The targeted near-IR photosensitizers pyrene-substituted bacteriochlorin (PyBac) and chlorin (PyChl) were then synthesized *via* the diimide reduction of pyrene–porphyrin, PyP (**8**), under microwave irradiation with a slight modification.[30] The main advantage of using microwave irradiation to synthesize near-IR photosensitizers over conventional heating was to reduce the reaction time and volume largely. Notably, PyChl (**9a**) and PyBac (**9b**) were obtained by the reduction of the precursor pyrene–porphyrin (**8**) and further reacted in the presence of *p*-toluene sulfonyl hydrazide and K_2CO_3 using a 1,4-dioxane solvent. The final products PyChl (**9a**) and PyBac (**9b**) were obtained with moderate yields of 19% and 22%, respectively.

The reaction parameters, such as temperature, duration, and concentration of the reactants, and work-up procedures were optimized for maximizing the yields of the near-IR photosensitizers (Table S1 in the ESI†). Pyrene–chlorin and pyrene–bacteriochlorin were isolated by column chromatography (Fig. S1, ESI†), and characterized by UV-vis, fluorescence, and mass spectroscopy [Fig. 1 (i), (ii), and Fig. S8, S9 in the ESI†]. The purity of all the photosensitizers (**7**, **8**, **9a**, and **9b**) was confirmed by HPLC analysis (Fig. S10–S14, ESI†).

Photophysical analysis of the pyrene-conjugated porphyrin, chlorin and bacteriochlorin

Absorption and fluorescence emission spectra. The tetrapyrrole-based porphyrin, chlorin, and bacteriochlorin photosensitizers were predominantly characterized by electronic absorption spectroscopy.[28,30] They showed an intense Soret band and Q-bands according to their conjugation and the presence of metal inside the macrocycle.[30] The Soret band, also known as the B-band, occurs due to the transition from the ground state to the second excited state ($S_0 \rightarrow S_2$), and the spectrum range is 380–500 nm and differs according to substitution on the β- or *meso*-position of porphyrin.[30] The Q-bands of the spectrum are situated in the range of 500–750 nm, resulting from the second transition to the first excited state ($S_0 \rightarrow S_1$).[30] The effect of the pyrene chromophore on the photophysical properties of PyP (**8**), PyChl (**9a**), and PyBac (**9b**) were investigated and compared (Fig. 1 and Table 1). Herein, pyrene–porphyrin (**8**) showed the characteristic Soret band at 418 nm and Q-bands at 571 and 625 nm with a molar extinction coefficient of 2100–2600 $(mM\ L)^{-1}\ cm^{-1}$. Pyrene conjugation in porphyrin contributed to two additional peaks, at 327 and 341 nm, and one Q-band appeared at a longer wavelength up to 625 nm [Fig. 1 (i)]. Interestingly, after diimide reduction, pyrene–chlorin (**9a**) exhibited an absorption band at 406 nm (blue-shift of the Soret band by 12 nm) and a characteristic peak (Q-band) at 624 nm. Notably, PyChl (**9a**) also showed two peaks, at 323 and 340 nm, with a blue-shift by 3 and 1 nm compared to PyP (**8**). PyChl showed the highest molar extinction coefficient [6800–8000 $(mM\ L)^{-1}\ cm^{-1}$; Table 1]. Similarly, pyrene–bacteriochlorin (**9b**) exhibited two Soret bands at 374 and 387 nm; and one additional peak was observed at 349 nm due to the pyrene ring, as well as a Q-band peak at 507 and characteristic peak at 730 nm together with a moderate molar extinction coefficient [3400–4000 $(mM\ L)^{-1}\ cm^{-1}$; Fig. 1 (i) and Table 1]. Compared with PyP (**8**), PyBac (**9b**) showed a strong red-shift of the pyrene group by 22 nm and a stronger bathochromic shifting, making it a promising candidate for bioimaging. The molar extinction

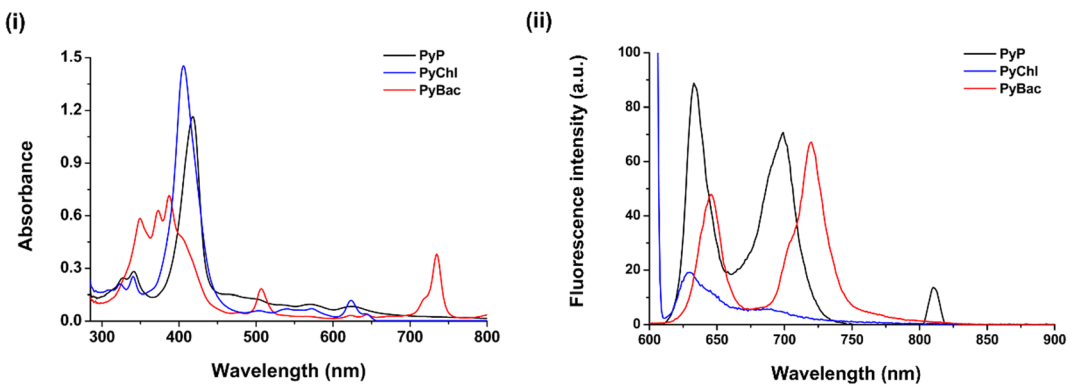

Fig. 1 (i) UV-vis spectra of pyrene-conjugated porphyrin (PyP; **8**), chlorin (PyChl; **9a**), and bacteriochlorin (PyBac; **9b**), (ii) fluorescence emission spectra of pyrene-conjugated porphyrin (PyP; **8**), chlorin (PyChl; **9a**), and bacteriochlorin (PyBac; **9b**).

Table 1 Photophysical properties of pyrene–porphyrin (**8**), pyrene–chlorin (**9a**), and pyrene–bacteriochlorin (**9b**)

PS	Stock solution (Colour)	λ_{max}/Molar extinction coefficient (ε) (mM L)$^{-1}$ cm^{-1}				Fluorescence (at 365 nm)	λ_{em} (nm)	Fluorescence quantum yield (Φ_F)*
		B-bands	Soret	Q_y-band	Q_x-band			
PyP (**8**)	Red	327 nm (2263.91) 341 nm (2563.63)	418 nm (2140.25)	571 nm (2633.08)	625 nm (2553.87)	Pink	632, 699, 810	0.55 ± 0.07
PyChl (**9a**)	Green	323 nm (7388.04) 340 nm (7286.86)	406 nm (6897.83)	—	624 nm (7906.23)	Dark pink	630	0.85 ± 0.12
PyBac (**9b**)	Pink	349 nm (3432.79)	374 nm (3430.79) 387 nm (3928.57)	507 nm (3455.99)	730 nm (3438.33)	Light pink	645, 735	0.66 ± 0.03

coefficient (ε) of each photosensitizer (**8**, **9a**, and **9b**) is also listed in Table 1.

The fluorescence study of **8**, **9a**, and **9b** was conducted at different excitation wavelengths. After analysis, they all showed emission within the phototherapeutic window (NIR-I window). Pyrene–porphyrin (**8**) displayed emission peaks at 632, 699, and 810 nm, while pyrene–chlorin showed a single emission peak at 630 nm, and pyrene–bacteriochlorin showed two peaks at 645 and 735 nm. Hence, all the photosensitizers emitted fluorescence around 630–750 nm, which is good for NIR fluorescence bioimaging.

Fluorescence quantum yield (Φ_F)

The fluorescence quantum yield is the key optical parameter to quantify a photosensitizer's ability to emit fluorescence upon excitation. The fluorescence quantum yields (Φ_F) of pyrene-conjugated porphyrin (**8**), chlorin (**9a**), and bacteriochlorin (**9b**) were determined by a steady-state comparative method, with reference to zinc phthalocyanine (ZnPc; in DMF). All the photosensitizers exhibited greater fluorescence quantum yields (Φ_F) than ZnPc (Φ_F = 0.3) due to the attachment of a fluorophore, *i.e.* pyrene. Among them, PyChl (**9a**) and PyBac (**9b**) showed higher values (Φ_F = 0.85 ± 0.12 and 0.66 ± 0.03) compared to porphyrin (Φ_F = 0.55 ± 0.07) (Table 1). Generally, the reduced double bond of the one and two pyrrole rings of the PyChl and PyBac structures alters the distortion and non-planarity in the macrocycle structure compared to the planar extensive π-conjugated porphyrin. Consequently, this reduces the non-radiative relaxation pathways, such as vibrational relaxation and internal conversion, which enhances the fluorescence efficiency of the NIR photosensitizers.

Computational analysis of the pyrene-conjugated porphyrin, chlorin, and bacteriochlorin

Density functional theory (DFT) and time-dependent DFT (TD-DFT) based computational calculations were carried out using the Gaussian 16 package.[37] The Gouterman four-orbital model (CAM-B3LYP) method and LANL2DZ basis set were utilized to study the electronic properties of the photosensitizers [PyP (**8**), PyChl (**9a**), and PyBac (**9b**)].[22,36,38] The optical and electronic properties of pyrene-conjugated porphyrin (**8**), chlorin (**9a**), and bacteriochlorin (**9b**) were compared. The frontier molecular orbitals, and HOMO and LUMO energy diagrams were observed to establish the correlation between the experimental and theoretical study findings. The delocalization of π-orbitals, *i.e.* HOMO and LUMO electrons, were situated mainly over the whole of the pyrrolic backbone. This did not change the general characteristics of the parent porphyrin, chlorin, and bacteriochlorin, but the pyrene ring donates electrons to the pyrrolic macrocycle, which results in the delocalization of HOMO electrons throughout the macrocycle.[36,38–40] Interestingly, electron density transfer from the bacteriochlorin macrocycle (PyBac) to the pyrene ring was seen in the LUMO+1 (Fig. 2). Pyrene–porphyrin was compared with the corresponding chlorin and bacteriochlorin. A previous study suggested that the reduction in the number of π-electrons in bacteriochlorin from 22 to 18 changes and narrows the HOMO–LUMO energy gap.[41] Consequently, the energy gap (HOMO–LUMO transition) of pyrene–porphyrin (**8**) was found to be higher (0.165 eV) than that of pyrene–chlorin (**9a**; 0.153 eV) and pyrene–bacteriochlorin (**9b**; 0.136 eV). The electronic transition (from the HOMO to LUMO+1) of pyrene–porphyrin (**8**) required higher energy (0.181 eV) compared to the corresponding chlorin (**9a**, 0.167 eV) and bacteriochlorin (**9b**, 0.173 eV). Pyrene-substitution in porphyrin exhibited the lowest energy level of LUMO+1, providing a longer wavelength of the Q-band at up to 625 nm, as could be observed in the UV-vis spectrum of pyrene–porphyrin (Fig. 1).

As reported in the previous literature, the origin of the Q-bands involves only HOMO−1, HOMO, LUMO, and LUMO+1 level transitions.[39] Herein, the present study revealed that the Q_x band (λ_{max} = 735 nm) of pyrene–bacteriochlorin (**9b**) mainly occurred due to the HOMO → LUMO transition and a small part of the next-HOMO → next-LUMO transition. The Q_y band of PyBac, which appeared at 507 nm, equally corroborated the HOMO−1 → LUMO and HOMO → LUMO+1 transitions. The B_x (Soret band) rose due to the HOMO → LUMO+1 electronic transition. Whereas the next B_y (next band) corresponded to the HOMO−1 to LUMO+1 transition. This induced a bathochromic (red-shift) and hyperchromic effect on the PyBac (**9b**) spectra (Fig. 1). In the pyrene–chlorin (**9a**) counterpart, the Q_x band was displayed at 624 nm (*i.e.* red region of the electromagnetic spectrum). The Q_x and Q_y bands of porphyrin were also observed at 625 and 571 nm, respectively. These electronic changes also raised the energy of the HOMO by changing its nature.[41] The photophysical changes of the photosensitizers had a strong effect on the oscillator strengths. PyBac (**9b**) showed the highest oscillator strength (*f*; 0.37) compared to pyrene–porphyrin (**8**; 0.03) and pyrene–

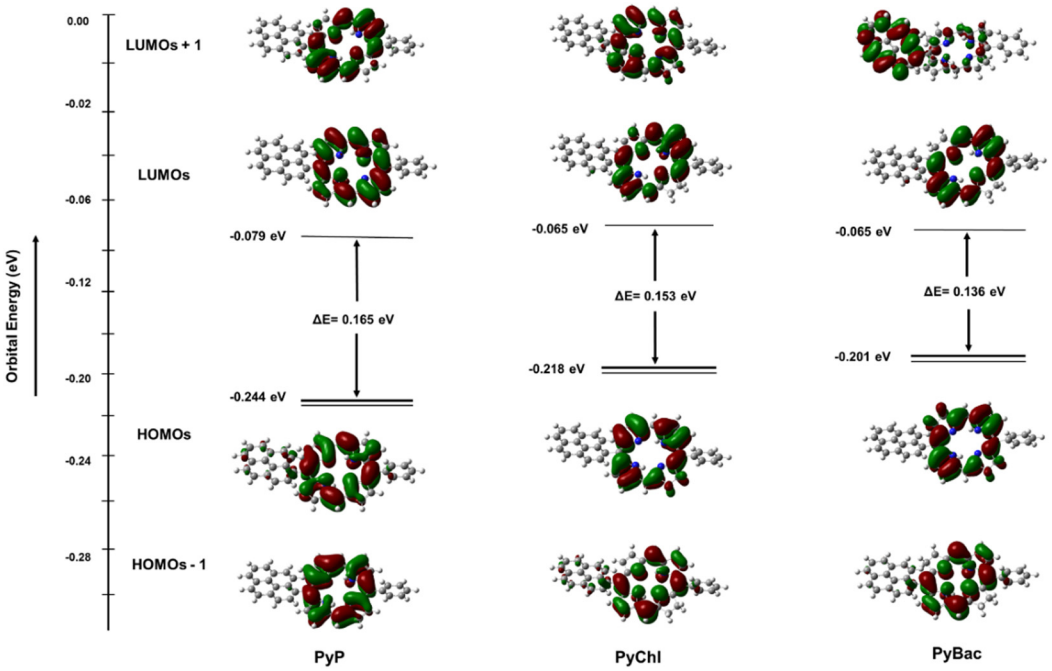

Fig. 2 Excited state geometries of pyrene-conjugated PyP (**8**), PyChl (**9a**), and PyBac (**9b**) obtained from TD-DFT calculations at the CAM-B3LYP/LANL2DZ level of theory.

Table 2 TD-DFT calculated excitation energies for HOMO- and LUMO-type molecular orbitals and the oscillator strengths (*f*)

Parameters	PyP	PyChl	PyBac
Electronic energy (Hartree)	−1833.62	−1834.80	−1836
HOMO−1	−0.247	−0.243	−0.241
HOMO	−0.244	−0.218	−0.201
LUMO	−0.079	−0.065	−0.065
LUMO+1	−0.063	−0.051	−0.028
Energy gap, (E_g) (HOMO–LUMO+1)	0.181	0.167	0.173
Energy gap, (E_g) (HOMO–LUMO)	0.165	0.153	0.136
Excited state 1	590 nm	637 nm	732 nm
Oscillator strength	0.0305	0.1757	0.370

chlorin (**9a**; 0.17), which was because a change in the transition dipole moment leads to an enhanced oscillator strength (*f*) [Table 2].

Conclusively, the TD-DFT study of the photosensitizers (**8**, **9a**, and **9b**) established the correlation between the experimental and theoretical calculations based on the photophysical parameters. The computed results also provided insights into the distribution of electrons within the HOMOs and LUMOs (Fig. 2).[39,41] In the case of pyrene–porphyrin (**8**), it was observed that the distinctive electronic transitions (from HOMO to LUMO; HOMO to LUMO+1) led to a shift of the Q_x band to the red region at 625 nm [Fig. 1(i)].

Fabrication and characterization of nanolignin sensitizers

Lignin, an aromatic macromolecule with a negative charge due to the presence of polyphenolic groups and their nanoparticles can be used as a nanocarrier to deliver hydrophobic photosensitizers.[21,42] The highly aromatic PyP (**8**) and NIR sensitizers [PyChl (**9a**) and PyBac (**9b**)] were doped in lignin nanoparticles *via* the solvent–antisolvent method.[21] Kraft lignin powder (20 mg mL^{-1}) was prepared in ethanol. Then, pyrene–porphyrin (**PyP**) and the NIR sensitizers (**PyChl** and **PyBac**) were dissolved in a saturated solution of ethanol–acetone (1:1). Both solutions were the mixed, and added to deionized water at a flow rate of 0.1 mL min^{-1}. The resulting mixture was subjected to sonication for 10 min. Then, the reaction was removed and centrifuged. The final pellet was diluted with deionized water and lyophilized to obtain a dried powder, which was utilized for further analysis (Fig. 3).

Mechanistically, the highly aromatic photosensitizer can attach to the lignin surface by electrostatic, hydrogen bonding, and π–π stacking, which provides certain advantages, including good stability and aqueous solubility.[21,43]

The mean particle size and surface zeta potential (for PyP-LNCs, PyChl-LNCs, and PyBac-LNCs) of the nanoformulations were initially measured using dynamic light scattering (DLS). The average particle size of the bare LNPs was ∼74 nm with a good polydispersity index of 0.17. After the encapsulation of each photosensitizer [PyP (**8**)/PyChl (**9a**)/PyBac (**9b**)], the average size of the nanoparticles (PyP-LNCs, PyChl-LNCs, and PyBac-LNCs) increased by ∼45 nm. The pyrene–porphyrin-loaded lignin nanoparticles (PyP-LNCs) were found to be ∼116 nm. With the encapsulation of the NIR sensitizers, the histogram of pyrene–chlorin-loaded LNCs (PyChl-LNCs) and pyrene–bacteriochlorin-loaded LNCs (PyBac-LNCs) exhibited ∼123 nm and ∼114 nm *Z*-averages, respectively (Fig. 4 and Table S2 in the ESI†). The surface charges of

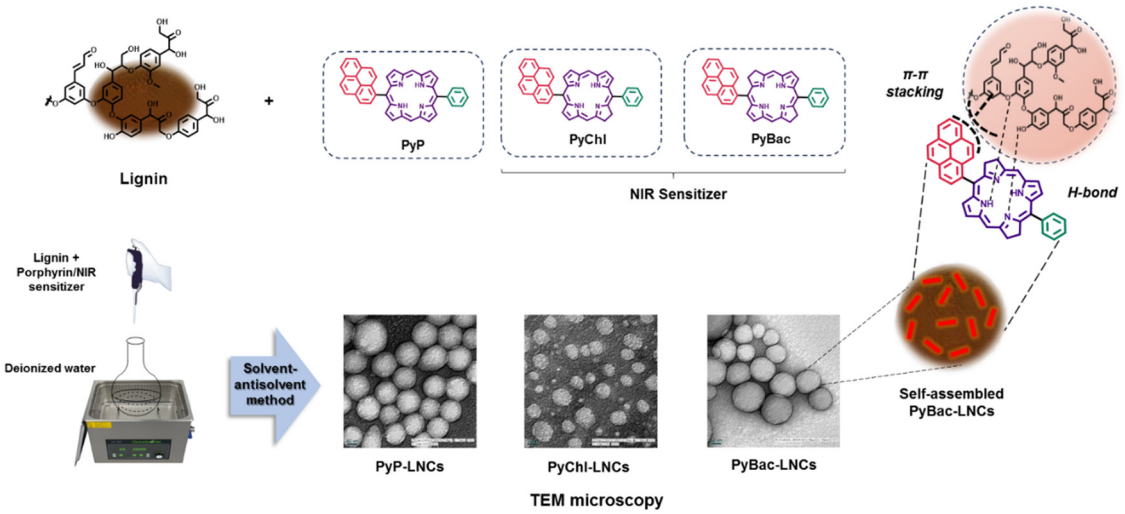

Fig. 3 Fabrication and characterization of pyrene–porphyrin, pyrene–chlorin, and pyrene–bacteriochlorin-loaded lignin nanoparticles (PyP-LNCs, PyChl-LNCs, and PyBac-LNCs).

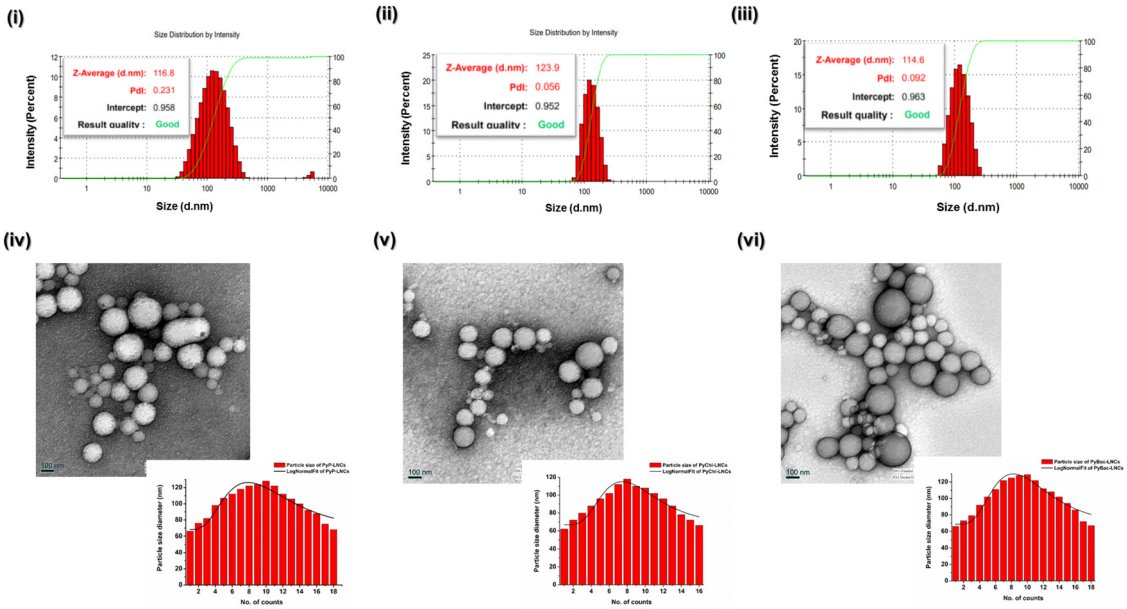

Fig. 4 Size-distribution histograms and corresponding transmission electron microscopy (TEM) images of the nanoparticles for (i), (iv) pyrene–porphyrin-loaded lignin nanoparticles (PyP-LNCs), (ii), (v) pyrene–chlorin-loaded lignin nanoparticles (PyChl-LNCs), and (iii), (vi) pyrene–bacteriochlorin-loaded lignin nanoparticles (PyBac-LNCs).

PyP-LNCs, PyChl-LNCs, and PyBac-LNCs nanoparticles were found to be ∼−31, ∼−29, and ∼−34 eV, respectively (Fig. S3 in the (ESI†) and Table 3). TEM images were obtained to provide information regarding the morphology and size of the nanoparticles. The nanolignin sensitizers (PyP-LNCs, PyChl-LNCs, and PyBac-LNCs) were found to be spherical in the size range of 100–130 nm (Fig. 4).

Spectroscopic analysis of the nanoformulations (PyP-LNCs, PyChl-LNCs, and PyBac-LNCs) was done to confirm the characteristics of the Soret peak and Q-bands. The pyrene–porphyrin-loaded lignin nanoparticles (PyP-LNCs) exhibited a Soret peak at 408 nm; while the pyrene–chlorin-loaded nanoparticles (PyChl-LNCs) showed the Soret peak at 421 nm. The spectroscopy analysis also confirmed the NIR peak of PyBac-LNCs at 753 nm [Fig. S16 (ii), ESI†]. These results indicated that the near-IR sensitizers retained their photophysical properties as intact post-nano entrapment.

Percentage (%) loading, pH-dependent release kinetics, and stability studies of the nanolignin sensitizers

In order to determine the efficacy of the nanolignin sensitizers as imaging probes, percentage loading, pH-dependence, and

Table 3 Singlet oxygen quantum yield (Φ_Δ) of pyrene-conjugated porphyrin, chlorin, and bacteriochlorin (**8**, **9a**, **9b**), their nanoformulations, and zinc phthalocyanine (ZnPc)[a]

Sample	Standard equation	Φ_Δ
PyP (**8**)	$y = -0.001x + 1.039$	0.30 ± 0.02
PyChl (**9a**)	$y = -0.0014x + 0.916$	0.41 ± 0.02
PyBac (**9b**)	$y = -0.0012x + 1.121$	0.36 ± 0.01
PyP-LNCs	$y = -0.0008x + 1.0097$	0.23 ± 0.01
PyChl-LNCs	$y = -0.0011x + 1.0201$	0.32 ± 0.02
PyBac-LNCs	$y = -0.001x + 0.9756$	0.29 ± 0.04
ZnPc	$y = -0.0019x + 0.9217$	0.56

[a] All the experiments were performed in triplicate.

stability studies were performed. In this line, the percentage loading of the developed pyrene–porphyrin and NIR sensitizers (pyrene–chlorin and pyrene–bacteriochlorin)-loaded lignin nanoparticles was determined using a previously reported method.[36,44] The loading efficiency of the nanoprobes, namely PyP-LNCs, PyChl-LNCs, and PyBac-LNCs, was found to be ~95%, ~90%, and ~91%, respectively (Fig. S17 and Table S3 in the ESI†).

The release kinetics pattern depends on the surrounding conditions of the diseased area, which could alter the efficiency and distribution of the photosensitizer molecule.[20] The release pattern, *i.e.* rapid or sustained release, plays a key role in systemic and cellular toxicity.[20] Here, a biological buffer system in acidic pH 5 and slightly basic 7.4 pH conditions was employed to assess the release patterns of PyP, PyChl, PyBac from PyP-LNCs, PyChl-LNCs, and PyBac-LNCs, respectively. The % cumulative release was determined using a UV-vis spectroscopic technique. The data revealed that PyP, PyChl, and PyBac had a rapid and sustained release over 24 h with percentage cumulative drug releases of 78 ± 3%, 79 ± 5%, and 84 ± 2%, respectively, at pH 5 (Fig. 5 and ESI,† Fig. S18). The cumulative drug release at pH 7.4 was 64 ± 7% for PyP-LNCs, 63 ± 6% for PyChl-LNCs, and 62 ± 2% for PyBac-LNCs (Fig. 5). Overall, it could be concluded that all the nanoparticles showed pH-responsive release kinetics, mimicking the acid nature of *Candida* fungal cells.

The stability study of the nanoformulations PyP-LNCs, PyChl-LNCs, and PyBac-LNCs was performed in terms of the mean particle size, polydispersity index, and surface charge of the nanoparticles. The nanoformulations were immersed in a buffer solution of pH 7, which was stored at 4 °C.[21] The above parameters were monitored at different time intervals and the nanolignin sensitizers were found to be stable for up to 3 months (Fig. S19, ESI†). Furthermore, the stability of nanoparticles was observed using TEM morphology analysis and their corresponding DLS data after one month. The size and morphology of each of the nanoformulations PyP-LNCs, PyChl-LNCs, and PyBac-LNCs were stable with *Z*-average sizes of 116, 129, and 115 nm, respectively (Fig. S20, ESI†).

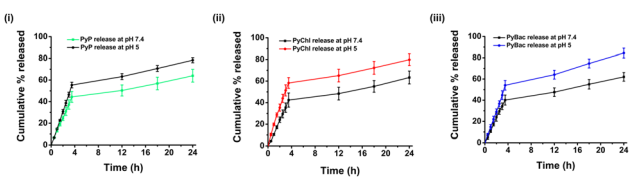

Fig. 5 Release kinetics study of the nanoformulations (PyP-LNCs, PyChl-LNCs, and PyBac-LNCs).

Singlet oxygen generation analysis

The reactive oxygen species (ROS) generation ability of a photosensitizer is a key parameter to determine its efficacy towards destroying microbes when activated by light. Therefore, the singlet oxygen quantum yield (Φ_Δ) of all the samples [PyP (**8**), PyChl (**9a**), PyBac (**9b**), PyP-LNCs, PyChl-LNCs, and PyBac-LNCs] was determined using the DPBF assay, with zinc phthalocyanine used as the standard. The highest singlet oxygen quantum yield was observed in the case of PyChl (0.41 ± 0.02) compared with the corresponding PyP (0.30 ± 0.02), PyBac (0.36 ± 0.01) under a green LED light (12 W; 500–570 nm, 32 400 J cm^{-2})/red LED light (12 W; 620–750, 32 400 J cm^{-2}), and using DMF as the solvent [Fig. S21 and Table 3]. Similarly, the NIR nanoprobes: PyChl-LNCs (0.32 ± 0.02) and PyBac-LNCs (0.29 ± 0.04) showed good quantum yields compared to the pyrene–porphyrin-loaded LNCs (PyP-LNCs; 0.23 ± 0.01) [Fig. 6 and Table 3]. Notably, the Φ_Δ values of the nanoprobes were relatively lower compared to their respective photosensitizers due to the restriction of light access to the photosensitizers in the aqueous medium. Other factors, such as polarity and the access to molecular oxygen by the nanoparticle matrix, may also play a key role in reducing the Φ_Δ values. The DPBF assay used in determining the Φ_Δ values involved a chemical probe named 1,3-diphenylisobenzofuran (DPBF). DPBF is a fluorescent molecule that acts as a singlet oxygen quencher, which reacts specifically with singlet oxygen and forms the non-fluorescent endoperoxide 1,2-dibenzoyl benzene irreversibly.[20,36,45]

Intracellular reactive oxygen species (ROS) determination

The generation of reactive oxygen species (ROS) by photosensitizers/nanophotosensitizers is crucial under light treatment during photodynamic and bioimaging applications.[46] Therefore, ROS generation quantification of the photosensitizers (**8**, **9a**, **9b**) and nanolignin sensitizers (PyP-LNCs, PyChl-LNCs, and PyBac-LNCs) was done using a DCFDA assay with a green LED (12 W; 500–570 nm, 32 400 J cm^{-2}) and red LED (12 W; 620–750 nm, 32 400 J cm^{-2}) respectively. The oxidation-sensitive DCFDA fluorescent probe was used to stain the fungal cells, followed by incubation with each sample treatment for 30 min (at 100 rpm; 37 °C). After incubation, the DCFDA was converted into non-fluorescent 2,7-dichlorofluorescein (DCFH2) in the presence of cellular esterase enzyme. DCFH2 further reacts with the ROS produced by the light-responsive photosensitizers/nanolignin sensitizers, which leads to the formation of highly fluorescent dichlorofluorescein (DCF) [Fig. 7(i)]. All the treatments were performed with different concentrations of 5, 10, and 15 μg mL^{-1}. The 5 and 10 μg mL^{-1} treatments were compared with their dark treatments, producing 2–5-fold higher ROS [Fig. S23, ESI†]. However, when the nanolignin sensitizers with 15 μg mL^{-1} dose were chosen, they

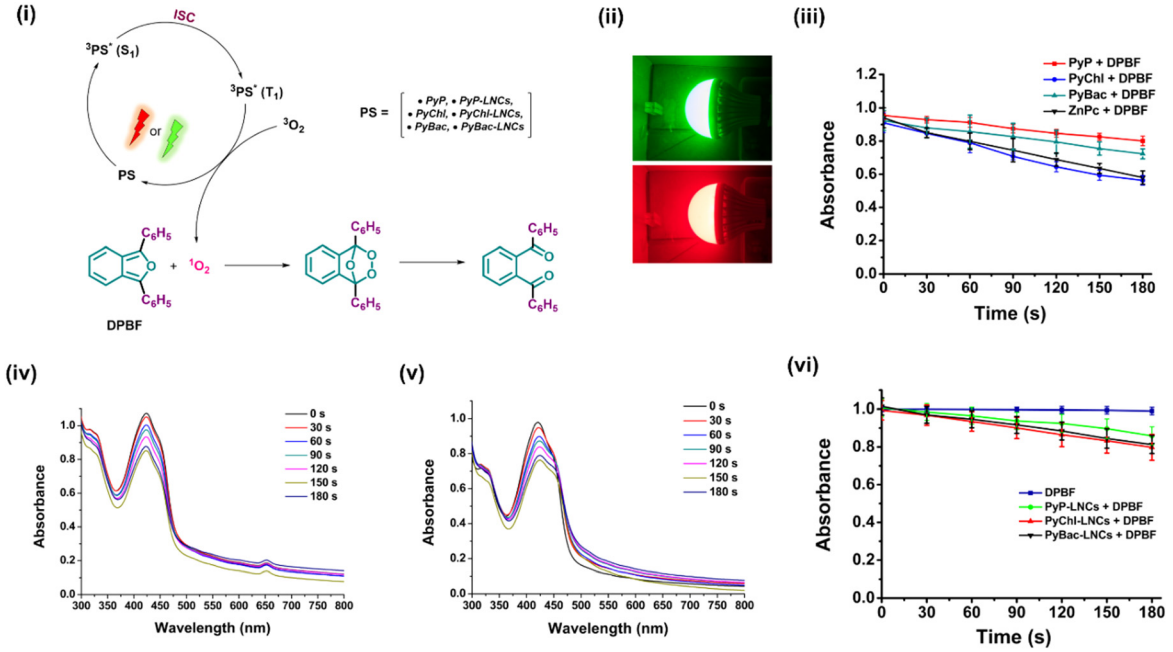

Fig. 6 (i) Mechanistic scheme showing the reaction of molecular oxygen with DPBF fluorescent dye, (ii) SOQY model depicting the cuvette containing the sample and the DPBF dye irradiated with green/red LED light, (iii) singlet oxygen production capability of PyP (**8**), PyChl (**9a**), and PyBac (**9b**) molecules measured by absorbance of quenched DPBF dye, (iv) DPBF absorbance upon 30 s time interval exposure with the PyChl-LNCs nanoprobe under the red LED light (12W), (v) DPBF absorbance upon 30 s exposure with the PyBac-LNCs nanoprobe under the red LED light (12 W), and (vi) singlet oxygen production capability of the nanoprobes PyP-LNCs, PyChl-LNCs, and PyBac-LNCs measured by the absorbance of DPBF.

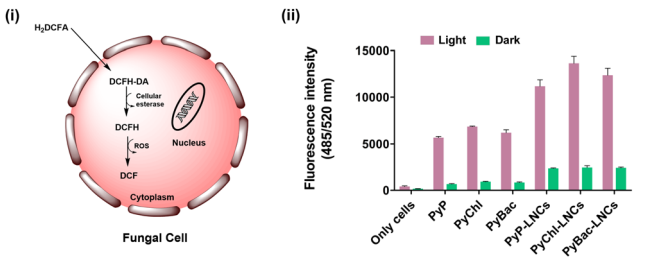

Fig. 7 (i) Conversion of dichlorodihydrofluorescein diacetate (DCFHDA) to dichlorofluorescein (DCF) inside the cells in the presence of esterase enzyme of *C. albicans*, (ii) ROS generation analysis with 15 μg mL^{-1} doses of the photosensitizers [PyP (**8**), PyChl (**9a**), and PyBac (**9b**)] and nanoformulations (PyP-LNCs, PyChl-LNCs, and PyBac-LNCs) under light and dark conditions.

showed up to a 12-fold higher ROS than their light-treated counterpart against fungal cells (*Candida albicans*) [Fig. 7(ii)]. Further, morphological deformities of the fungal cell walls were observed due to ROS production by the nanolignin sensitizers, as depicted in the SEM analysis (Fig. S22, ESI†). Overall, the nanolignin sensitizers are promising ROS generators for the eradication of microbes as exemplified by their effect on fungal cells.

DNA-intercalation study using the nanolignin sensitizers

The DNA binding analysis is crucial for studying preliminary biological responses. Determining DNA intercalation helps with the initial drug-development process. It was previously reported that the pyrene group binds with DNA and shows excellent DNA intercalation properties.[46,47] The planar structure of pyrene helps its insertion inside DNA base pairs, *i.e.* intercalation. The polypyrrole macrocycle could also help the non-covalent interactions, such as H-bonding and van der Waals forces, stabilize the photosensitizer–DNA complex.[44] Herein, to study DNA intercalation by the photosensitizers [PyP (**8**), PyChl (**9a**), and PyBac (**9b**)] and their nanoformulations (PyP-LNCs, PyChl-LNCs, and PyBac-LNCs), gel electrophoresis was performed using plasmid DNA pUC19. The results indicated that the photosensitizers bind/intercalate with DNA, as depicted by the hindrance in the movement of the DNA plasmid pUC19 (Fig. 6). Interestingly, all the pyrene-conjugated pyrrolic photosensitizers [PyP (**8**), PyChl (**9a**), and PyBac (**9b**)] showed the DNA intercalation property. Among these, pyrene–bacteriochlorin (**9b**) was found to be a very efficient DNA intercalator compared to EtBr. All the nanoformulations (PyP-LNCs, PyChl-LNCs, and PyBac-LNCs) also demonstrated DNA-intercalation capabilities, as shown in Fig. 8, Lanes 4, 5, and 6, respectively. Hence, the NIR fluorescent dyes (**8**, **9a**, **9b**) and their nanoformulations (PyP-LNCs, PyChl-LNCs, and PyBac-LNCs) can be used for DNA intercalation. Moreover, the effect of DNA binding on the photosensitizers was also examined by UV-vis and fluorescence spectroscopy. DNA pUC19 showed absorption around 260 nm.[48,49] After binding with each photosensitizer, a hypochromic shift of the DNA peak was observed. After DNA binding, the UV-vis

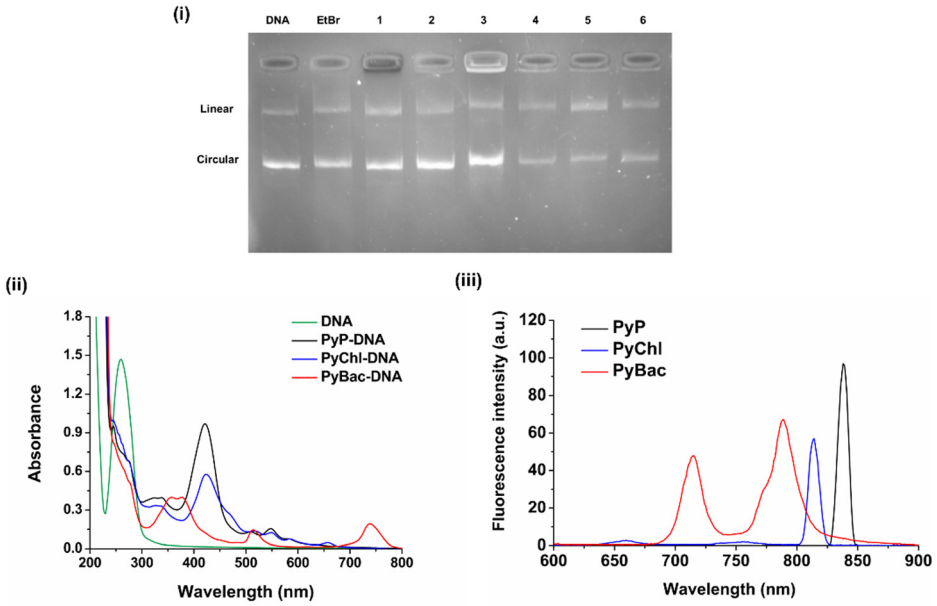

Fig. 8 DNA-intercalation study: (i) gel electrophoresis of genomic DNA pUC19; the treatment of EtBr was used as a reference to show DNA intercalation; lanes 1, 2, and 3 depict the DNA intercalation in the presence of PyP, PyChl, and PyBac, respectively, lanes 4, 5, and 6 indicate DNA intercalation in the presence of PyP-LNCs, PyChl-LNCs, and PyBac-LNCs, respectively, (ii) UV-vis spectra of the photosensitizers [PyP (**8**), PyChl (**9a**), and PyBac (**9b**)] after the DNA-intercalation study, and (iii) fluorescence emission spectra of the photosensitizers [PyP (**8**), PyChl (**9a**), and PyBac (**9b**)] after the DNA intercalation study.

spectrum of pyrene–porphyrin showed a hypochromic shift and red-shift by 3 nm from 418 nm to 421 nm. Pyrene–chlorin also exhibited hypochromic and red-shifted peaks: the Soret peak from 406 nm to 423 nm and Q-band from 630 nm to 657 nm. Meanwhile, pyrene–bacteriochlorin also showed hypochromic and red-shifts from 349 to 357 nm and 374 to 376 nm. The DNA intercalation of the photosensitizers (**8**, **9a**, and **9b**) was also monitored by the fluorescence intensity (Fig. 8(ii) and (iii)). In this study, PyP exhibited a fluorescence emission peak at 837 nm upon excitation at 418 nm. PyChl showed the emission at 814 nm upon 406 nm excitation. Meanwhile, PyBac displayed two emission peaks at 715 and 789 nm through 507 nm excitation. Conclusively, the spectroscopic study suggested that the DNA binding of each photosensitizer (**8**, **9a**, and **9b**) could bring photophysical changes (bathochromic and hypochromic shifts) due to intercalation.

Ethidium bromide (EtBr) and 4′,6-diamidino-2-phenyl-indole (DAPI) displacement study

Furthermore, the DNA-intercalation study findings were validated by an EtBr and DAPI displacement study.[50,51] The basic mechanism of the study was the competition between the DAPI/EtBr and the photosensitizer samples (**8**, **9a**, and **9b**).[50] The decrease in the fluorescence intensity of DAPI/EtBr after displacement by the photosensitizer sample confirmed their DNA-intercalation properties. Naturally, DNA does not possess fluorescence.[50,51] Therefore, two fluorophores, namely EtBr and DAPI, were combined to create pUC19(DNA)-EtBr (intercalator/binder) and pUC19(DNA)-DAPI (groove binder) adducts, respectively. After the addition of each of PyP, PyChl, and PyBac to the EtBr-DNA/DAPI-DNA adduct, the fluorescence intensity was found to be significantly reduced [Fig. 9 (i) and (ii)]. This fluorescence quenching indicated that each photosensitizer strongly displaced the EtBr and DAPI from the binding site present in the DNA (pUC19). Consequently, it provided strong evidence of the DNA-binding abilities of the designed photosensitizers: PyP, NIR-absorbing PyChl, and PyBac. The quenching constant (K_q) was calculated using the Stern–Volmer equation for each sample (Table 4):

$$F_0/F = K_q[Q] + 1 \quad (1)$$

where F_0 and F are the fluorescence emission intensities in the absence and presence of the photosensitizer sample, and $K_q[Q]$ is the quenching constant. According to the obtained values of the quenching constant, all the samples (**8**, **9a**, and **9b**) showed a higher association with DNA with major grooves and moderate intercalation (Fig. 9 and Table 4).

In vitro fluorescence imaging using the nanolignin sensitizers

Fungus, such as *Candida albicans*, can cause skin infections, and the overgrowth of this species causes candidiasis.[52,53] The development of resistance to antifungal medications has been found to be ineffective.[54,55] The major reason for the inefficacy in the treatment is due to the lack of detection of such fungi. In this line, bioimaging studies of the nanolignin sensitizers, namely PyP-LNCs, PyChl-LNCs, and PyBac-LNCs, were conducted on *Candida albicans* fungal cells. The *Candida* cells were stained by 4′,6-diamidino-2-phenyl-indole (DAPI, blue

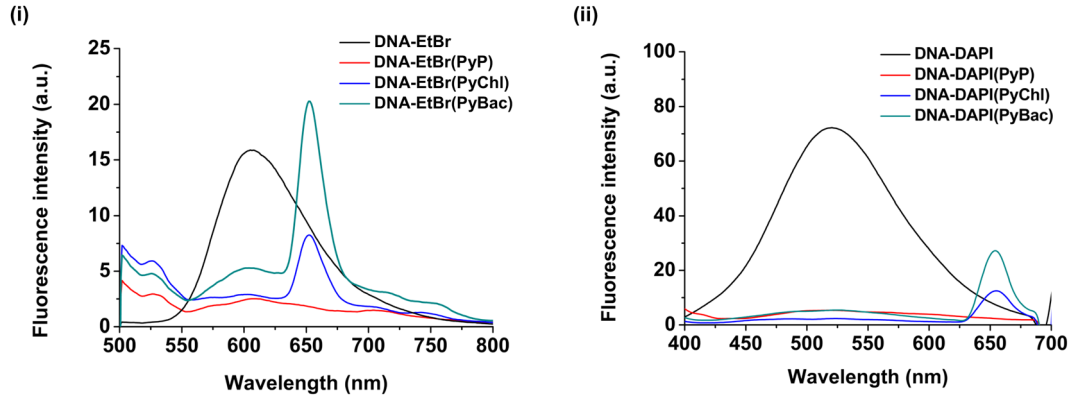

Fig. 9 Fluorescence quenching of (i) EtBr-DNA and (ii) DAPI-DNA adducts after displacement study by the photosensitizers [PyP (**8**), PyChl (**9a**), and PyBac (**9b**)] after DNA for determination of the quenching constant (K_q).

Table 4 Quenching constants (K_q) of the PyP, PyChl, and PyBac photosensitizers calculated using the Stern–Volmer equation (1)

Sample	K_q[Q] for EtBr	K_q[Q] for DAPI
PyP (**8**)	6.10 M^{-1}	12.46 M^{-1}
PyChl (**9a**)	4.51 M^{-1}	35.11 M^{-1}
PyBac (**9b**)	2.06 M^{-1}	12.79 M^{-1}

fluorescent stain) and were then incubated with each nanoprobe (PyP-LNCs, PyChl-LNCs, and PyBac-LNCs; Fig. 10). The fluorescence imaging was performed using an inverted fluorescence microscope (Fig. 8). In the study, the treated cells were excited with a wavelength of 525 nm, and the dark field images showed the red-light emission due to the pyrene–porphyrin, pyrene–chlorin, and pyrene–bacteriochlorin, as shown in Fig. 10 (ii)–(iv) respectively. The nanosensitizers were also compared with untreated/control cells [Fig. 10 (i) bright field, (ii) control cells in the dark field, and (iii) DAPI-treated control in the dark field] to prove their efficacy. To note, the pyrene–porphyrin, pyrene–chlorin, and pyrene–bacteriochlorin-based nanosensitizers entered the cells, possibly *via* passive diffusion.[48,49] Interestingly, the pyrene–porphyrin LNCs and pyrene–chlorin LNCs exhibited greater red emission compared to PyBac-LNCs. The nanosensitizers showed the binding with the *Candida albicans* cell membrane and the cytoplasm (Fig. 8). This indicated that the lignin nanoparticles could be a good drug-delivery carrier for the photosensitizers [PyP (**8**), PyChl (**9a**), and PyBac (**9b**)] for bioimaging purposes.

In vitro photoinactivation study of *Candida albicans* by PyP, PyChl, PyBac and their nanoformulations

The photodynamic inactivation of *Candida albicans* was tested to investigate the antimicrobial PDT potential of the photosensitizers [PyP (**8**), PyChl (**9a**), and PyBac (**9b**)] and their nanoformulations (PyP-LNCs, PyChl-LNCs, and PyBac-LNCs). The cell viability of these samples was evaluated based on the colony-forming units (CFUs) on the Yeast Peptone Dextrose (YPD) Agar Plates. After the incubation of each sample with *C. albicans*, they were subjected to dark and light (LED) treatments. The treated cells [with pyrene–porphyrin (PyP) and their nanoformulation (PyP-LNCs)] were irradiated under a green LED (12 W; 500–570 nm, 32 400 J cm^{-2}) light, while pyrene–chlorin (PyChl), pyrene–bacteriochlorin (PyBac), and their nanoformulations (PyChl-LNCs and PyBac-LNCs) were irradiated under a red LED (12 W; 620–750 nm) light. Each nanoformulation was taken as 0, 5, 10, 15, 20, and 25 μg doses. After 36 h incubation, the CFUs were counted after incubation and the % cell viability [Fig. 11] was calculated. Each sample set produced the IC_{50}, as demonstrated using a standard calibration plot drawn at 5, 10, 15, 20 and 25 μg mL^{-1} (Fig. 11 and Table 5).

The light treatment of each photosensitizer [PyP (**8**), PyChl (**9a**) and PyBac (**9b**)] produced up to 62–87% inhibition at 25 μg mL^{-1} concentration ($P > 0.001$) compared to the positive control, as shown in Fig. 11 (i). The IC_{50} of the PyBac (**9b**) photosensitizer was found to be very effective (IC_{50}:0.012 μM) compared to the IC_{50} of PyP (**8**) and PyChl (**9a**) with 0.025 μM and 0.017 μM doses, respectively (Table 5). Consequently, PyBac was found to have 2 and 1.4 times more potential than PyP and PyChl under light conditions [Fig. 11 (iii) and Fig. S21, ESI†]. Similarly, under the dark conditions for the treatments, they could inhibit the *Candida* cells by 47–51% (Fig. 11 (i)). Furthermore, their nanolignin sensitizers (PyP-LNCs, PyChl-LNCs, and PyBac-LNCs) increased the % inhibition by 81–92% at a 25 μg mL^{-1} concentration ($P > 0.001$) under light treatment [Fig. 11 (iii)]. The % cell viability data revealed that the nanolignin sensitizers of the respective photosensitizer were very effective against *Candida albicans* cells. Hence, the IC_{50} values of the nanolignin sensitizers PyP-LNCs, PyChl-LNCs, and PyBac-LNCs were observed at 9.42, 5.19, and 5.35 μg mL^{-1}, which were 1.3, 1.5, and 2 times less compared with PyP, PyChl, and PyBac, respectively (Table 5). Moreover, the antifungal PDT study using the nanolignin sensitizers demonstrated, improved hydrophilicity, leading to the enhanced effectiveness of the hydrophobic photosensitizers during antimicrobial photodynamic activity (Fig. 11), and the destruction of *Candida* cells could also be observed after each nanolignin sensitizer treatment (Fig. S22, ESI†).

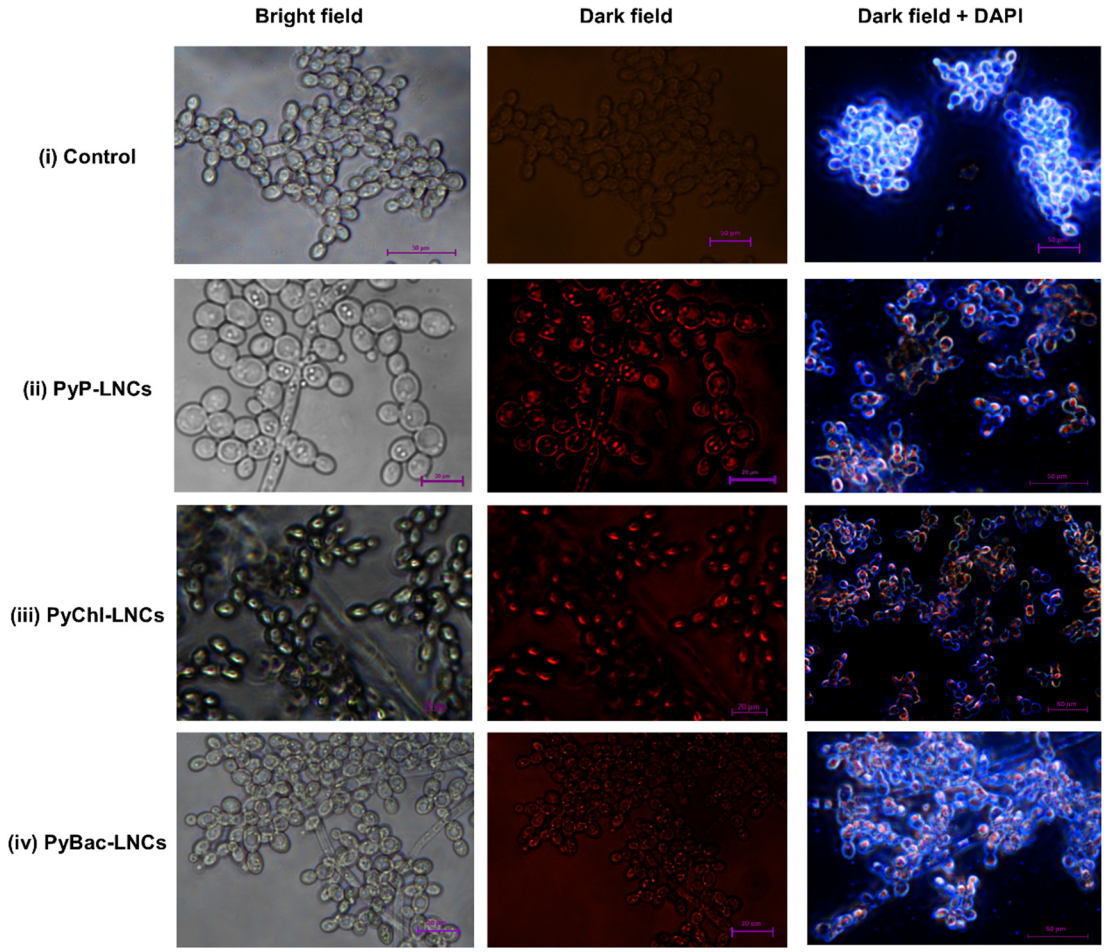

Fig. 10 *In vitro* fluorescence imaging study using DAPI: (i) Only *Candida albicans* cells/control in a bright field, without DAPI, and with DAPI, (ii) *C. albicans* incubation with PyP-LNCs (10 μg mL^{-1}) in a bright field, dark field, and dark field with DAPI (iii) incubation with PyChl-LNCs (10 μg mL^{-1}) in a bright field, dark field, and dark field with DAPI (iv) incubation with PyBac-LNCs (10 μg mL^{-1}) in a bright field, dark field, and dark field with DAPI.

Experimental section

Synthesis and characterization of pyrene-conjugated porphyrin, chlorin, and bacteriochlorin and their intermediates

***meso*-Pyrene dipyrromethane (3)/*meso*-phenyl dipyrromethane (5).** The existing method was followed with a few modifications to synthesize dipyrromethanes (DPM).[33] Pyrrole (14 mL, 2 mmol, 100 eq.) and 1-pyrene–carboxaldehyde (460 mg, 2 mmol, 1 eq.)/benzaldehyde (0.8 mL, 8 mmol, 1 eq.) were the starting materials for the synthesis of DPMs. They were added in RBF, followed by purging and reaction for 15 min. Then, indium chloride (44 mg; 2 mmol, 0.1 eq.) was added with constant stirring. Afterwards, the mixture of pyrrole and 1-pyrene–carboxaldehyde was heated at 75 °C for 3 h with constant stirring. Then, 2.4 g (30 eq.) of sodium hydroxide was added to the reaction mixtures (**3**) and stirred for 1 h. To synthesize *meso*-phenyl dipyrromethane (**5**), the mixture of pyrrole and benzaldehyde was stirred at room temperature for 15 min. Then, indium chloride was added and stirred at room temperature for 3 h. Both the resulting reaction mixture were separately purified by column chromatography using an EtOAc : *n*-hexane (1 : 9) solvent system and silica gel (100–200 mesh size). The yields of compounds **3** and **5** were calculated to be 68% and 61%, respectively. (Compound **3**) Yellow solid crystals: ^{1}H NMR. (500 MHz, DMSO-d_6) δ: 5.64 (d, J = 10 Hz, 2H), 5.94 (d, J = 5 Hz, 2H), 6.53 (s, 1H, R3H), 6.66 (d, J = 5 Hz, 2H), 7.72 (s, 1H, ArH), 8.04 (d, 15 Hz, 2H, ArH), 8.17 (d, 5 Hz, 2H, ArH), 8.20 (d, 10 Hz, 2H, ArH), 8.26 (s, 1H, ArH), 8.47 (s, 1H, ArH), 9.97 (d, 2H, NH) ppm; ^{13}C NMR. (125 MHz, $CDCl_3$) δ: 106.85, 106.97, 116.88, 123.41, 124.17, 124.74, 124.83, 125.07, 126.08, 126.70, 127.14, 127.39, 127.80, 129.38, 130.20, 130.82, 133.16, 137.83. HPLC-MS: ($C_{25}H_{18}N_2$) m/z $[M]^+$ calc. 346.15; found 346.15, m/z $[M-1]^+$ found 345.16.

1,9-Diformyl-5-(4-phenyl)dipyrromethane (6). The 1,9-formyl-5-(4-phenyl)dipyrromethane (**6**) was synthesized using the reported method with modifications.[34] Vilsmeier reagent was prepared *in situ* by mixing phosphorous oxychloride (1.1 mL, 5 mmol, 2.4 eq.) in 5 mL DMF solvent under inert conditions and at 0 °C. Then, *meso*-phenyl dipyrromethane [**5**(1.1 g, 5 mmol, 1 eq.)] was dissolved in DMF (5 mL) at 0 °C under inert conditions and stirred for 2 h. After completion of the reaction, a saturated aqueous solution of sodium acetate

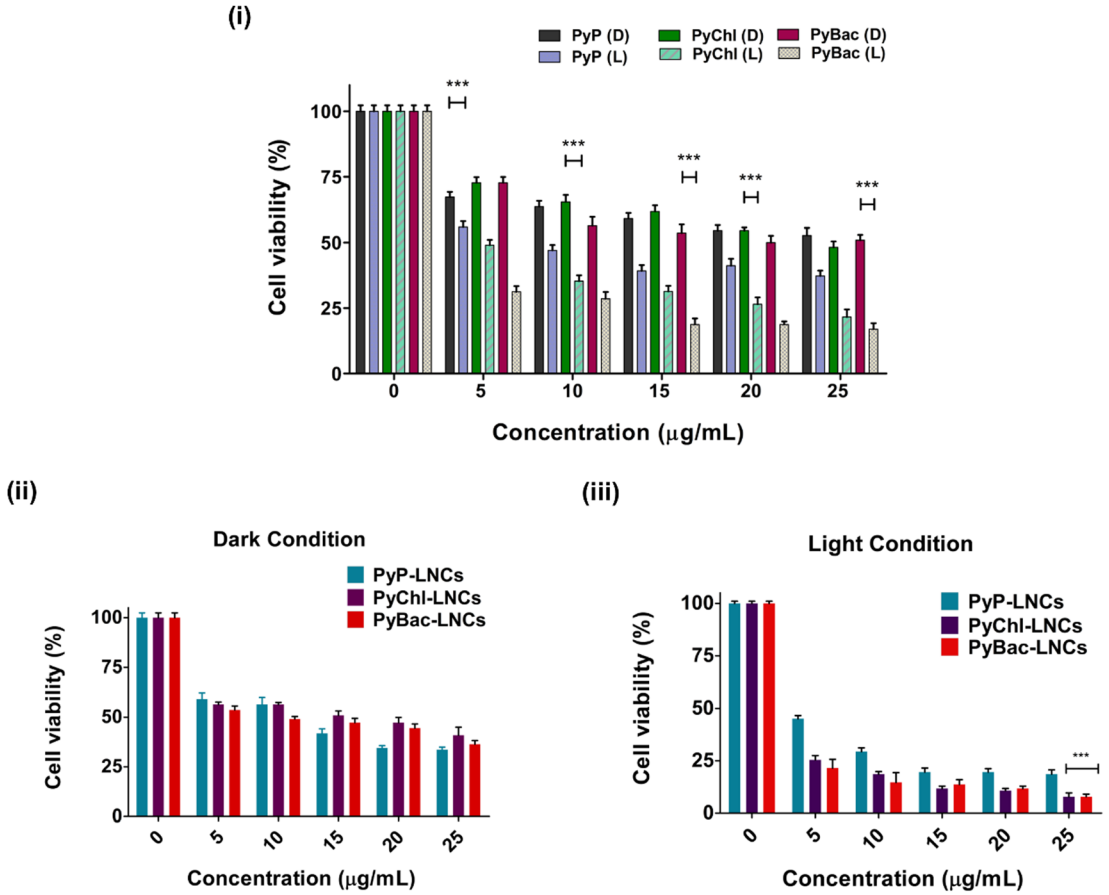

Fig. 11 Antimicrobial photodynamic activity: (i) the % cell viability of the nano lignin sensitizers in the dark, (ii) the % cell viability of the nano lignin sensitizers in the light treatments, (iii) the % cell viability of the photosensitizers: pyrene–porphyrin (PyP), pyrene–chlorin (PyChl) and pyrene–bacteriochlorin (PyBac) [*** depicts $P < 0.001$] and [** depicts $P < 0.01$].

Table 5 IC_{50} doses of the PyP, PyChl, PyBac photosensitizers and their nanolignin sensitizers (PyP-LNCs, PyChl-LNCs, and PyBac-LNCs) calculated after antimicrobial photodynamic therapy[a]

Sample	IC_{50} in dark condition (dose in μg)	IC_{50} in dark condition (dose in μM)	IC_{50} in light condition (dose in μg)	IC_{50} in light condition (dose in μM)	Fold reduction of doses (dark *vs.* light)
PyP (**8**)	28.97 ± 3.31	0.038 ± 0.05	14.74 ± 0.6	0.025 ± 0.001	2
PyChl (**9a**)	21.52 ± 0.41	0.036 ± 0.001	10.21 ± 0.22	0.017 ± 0.001	2.1
PyBac (**9b**)	20.56 ± 0.35	0.034 ± 0.001	7.26 ± 0.17	0.012 ± 0.001	2.8
PyP-LNCs	13.84 ± 0.42	—	9.42 ± 0.92	—	1.5
PyChl-LNCs	14.27 ± 2.82	—	5.19 ± 0.14	—	2.7
PyBac-LNCs	13.72 ± 1.37	—	5.35 ± 0.6	—	2.5

[a] All the experiments were conducted in triplicate.

was added and the resulting mixture was transfer at room temperature. The resulting mixture was then extracted with ethyl acetate and washed with brine three times. The organic layer was collected, dried using sodium sulfate, and concentrated. The resulting brown semisolid product (**6**) was loaded on silica gel and purified by column chromatography using an EtOAc : *n*-hexane solvent system (1 : 9). The brownish solid product was obtained (680 mg, 49%). The product was characterized by ^{1}H-NMR spectroscopy and the data were found to be consistent with a previous report.[36]

Zn(II)-5-[4-pyrene]-15-(4-phenyl)porphyrin (7). The synthesis of ZnPyP (7) was performed using the classic MacDonald-type method with some modifications.[32,56] The starting materials 1,9-diformyl-5-(4-phenyl)dipyrromethene (**6**) (563 mg, 1.62 mmol, 1 eq.) and *n*-propylamine (8 mL, 1.62, 3.45 eq.) were dissolved in THF and stirred for 1 h. After imine formation, the excess *n*-propylamine and THF solvent were removed by *in vacuo* evaporation. The resulting crude reaction mixture was dissolved in ethanol (50 mL), followed by the addition of *meso*-pyrene–dipyrromethane (**3**) and zinc acetate (3.5 g, 5 mmol, 10 eq.), and then refluxed at 78 °C for 13 h.

The reaction was monitored by TLC. After completion of the reaction, filtered with ethyl acetate on a sintered glass funnel containing neutral alumina. The Zn(II) pyrene–porphyrin (**7**) was isolated (25% yield) by column chromatography using silica gel G, using EtOAc : *n*-hexane (1 : 9) as the solvent system. Red solid crystal was found, ESI-MS: *m*/*z* $[M + 1]^+$ calc. for $C_{42}H_{24}N_4Zn$: 649.13; found 649.16. HPLC analysis, t_R = 10.86 [the analysis was performed isocratically in 0.1% TFA in an acetonitrile and water composition (90:10) run over 20 min, purity >99%].

5-[4-Pyrene]-15-(4-phenyl)porphyrin (8). A previously reported method was followed for the demetallation of ZnPyP (**7**; 0.24 mmol),[32,56] in which compound (**7**) was dissolved in anhydrous DCM. Then, TFA was added and stirred for 5 h at room temperature. This reaction was then monitored by TLC. After the completion of the reaction, the mixture was poured into an aqueous sodium bicarbonate solution to neutralize the excess TFA. Pyrene–porphyrin (PyP, **8**) was obtained as a dark red solid (142 mg, 99% yield); ^{1}H NMR (500 MHz, $CDCl_3$) δ: −3.02 (s, 2H, NH), 4.12 (d, J = 10 Hz, 2H), 7.42 (s, 1H), 7.44 (s, 1H), 7.67 (s, 1H), 7.68 (s, 1H), 7.81 (s, 1H), 7.83 (s, 1H), 8.09 (s, 1H), 8.10 (s, 1H), 8.32 (s, 1H), 8.34 (s, 1H), 8.43 (s, 1H), 8.56 (s, 1H), 8.71 (s, 1H), 8.77 (s, 1H), 8.85 (s, 1H), 9.10 (s, 1H), 9.16 (s, 1H), 9.27 (s, 1H), 9.32 (s, 1H), 9.40 (s, 1H), 10.30 (d, 2H) ppm. λ_{max} (abs.: 327, 341, 418, and 625 nm), λ_{max} (em.: 632, 699, and 810 nm), ESI-MS: *m*/*z* $[M + 1]^+$ calc. for $C_{42}H_{26}N_4$: 586.22; found 587.27. HPLC analysis, t_R = 27.18 [the analysis was performed isocratically in 0.1% TFA in an acetonitrile and water composition (90:10) run over 60 min, purity >99%].

5-[4-Pyrene]-15-(4-phenyl)chlorin (9a) and 5-[4-Pyrene]-15-(4-phenyl)bacteriochlorin (9b). A previously reported synthetic method with a few modifications was utilized to construct pyrene–bacteriochlorin.[30] The precursor pyrene–porphyrin (10 mg, 0.017 mmol, 1 eq.) was taken in a microwave reaction vial. Then, anhydrous K_2CO_3 (234 mg, 1.7 mmol, 100 eq.) and *p*-toluene sulfonyl hydrazide (317 mg, 1.7 mmol, 100 eq.) were added to it, followed by the addition of 1,4-dioxane solvent (3 mL). Next, the microwave reaction was performed at 130 °C for 25 min. The reaction was observed by TLC and UV-vis spectroscopy. Two products were identified, namely pyrene–chlorin (**9a**) and pyrene–bacteriochlorin (**9b**). The reaction mixture was then poured into water, and the products were extracted using DCM as the solvent. The resulting mixture was then passed through a bed of alumina. Both compounds were then isolated by column chromatography (silica, DCM:petroleum ether, 1:3).

5-[4-Pyrene]-15-(4-phenyl)chlorin (9a). Light green solid (2 mg, 19%); ^{1}H NMR (500 MHz, $CDCl_3$) δ: −2.99 (d, 2H, NH), 3.46 (s, 1H), 4.12 (d, J = 10 Hz, 2H), 4.67 (s, 1H), 5.29 (m, 3H), 5.81 (s, 1H), 6.59 (s, 1H), 6.98 (s, 1H), 7.43 (s, 1H), 7.68 (s, 1H), 7.70 (s, 1H), 7.82 (m, 3H), 8.57 (s, 1H), 8.72 (s, 1H), 8.86 (s, 1H), 9.11 (s, 1H), 9.17 (s, 1H), 9.29 (s, 1H), 9.41 (s, 1H), 9.34 (s, 1H), 10.32 (d, 2H) ppm. λ_{max} (abs.: 323, 340, 406, and 624 nm), λ_{max} (em.: 630 nm), ESI-MS: *m*/*z* $[M]^+$ calc. for $C_{42}H_{28}N_4$: 588.24; found 588.23 and $[M+1]^+$ found 589.28. HPLC analysis, t_R = 2.89 [the analysis was performed isocratically in 0.1% TFA in an acetonitrile and water composition (90:10) run over 20 min, purity >99%].

5-[4-Pyrene]-15-(4-phenyl)bacteriochlorin (9b). Light red solid (2.5 mg, 22%); ^{1}H NMR (500 MHz, DMSO-d_6) δ: −3.16 (d, 2H, NH), 3.40 (d, 2H), 3.47 (d, 2H), 3.92 (m, 4H), 4.88 (m, 4H), 5.72 (s, 1H), 6.86 (s, 1H), 7.25 (s, 1H), 7.81 (s, 1H), 8.12 (s, 1H), 8.48 (s, 1H), 8.64 (s, 1H), 9.03 (s, 1H), 9.53 (d, J = 5 Hz, 2H), 9.65 (d, J = 5 Hz, 2H), 10.62 (s, 1H), 10.93 (s, 1H), 12.30 (d, 2H) ppm. λ_{max} (abs.: 323, 349, 374, 507 and 730 nm), λ_{max} (em.: 645, and 735 nm), ESI-MS: *m*/*z* $[M]^+$ calc. for $C_{42}H_{30}N_4$:590.25; found 590.29, *m*/*z* $[M+1]^+$ found 591.30. HPLC analysis, t_R = 8.72 [the analysis was performed isocratically in an acetonitrile and water composition (95:5) run over 20 min, purity >98%].

Photophysical analysis. Absorption and fluorescence emission spectra are described in the ESI.†

Molar absorption coefficient (ε). The ε of each photosensitizer (PyP, PyChl, and PyBac) was calculated using DMF solvent. The B-band, Soret peak, and the Q-bands of each photosensitizer were observed in their UV-vis spectra. They were calculated using the following equation for the ε value:

$$\varepsilon = A/c{\cdot}l \quad (2)$$

where ε is the molar absorption coefficient, A is the absorbance, c is the molar concentration, and l is the path length of the respective photosensitizer.

Fluorescence quantum yield (Φ_F)

The Φ_F yields were recorded by a fluorescence spectrophotometer using a comparative method with zinc phthalocyanine in DMF solvent as a reference (Φ_F = 0.3; Table S4, ESI†). The following standard equation was used for the calculation of Φ_F:

$$\Phi_{F(u)} = \Phi_{F(ref)} \times I_u/I_{ref} \times A_{ref}/A_u \times \eta_u{}^2/\eta_{ref}{}^2 \quad (3)$$

where Φ_F is the fluorescence quantum yield, I is the integrated fluorescence intensity, A is the absorbance at the excitation wavelength, and η represents the refractive index of the solvents used for the samples and references. The subscripts u and ref denote unknown and reference, respectively.

Molecular orbital calculations

Time-dependent density functional theory (TD-DFT) calculations were performed with the CAM-B3LYP method and LANL2DZ basis set, and the equilibrium geometries were fully optimized using the same parameters.[37,38,40]

Development of lignin nanoparticles (LNPs) and pyrene-based porphyrin and NIR photosensitizers-loaded lignin nanoparticles

The PyP-LNCs, PyChl-LNCs and PyBac-LNCs were prepared according to previous publications with minor modifications.[21] A stock solution of Kraft lignin (20 mg mL^{-1}) was prepared in ethanol. On the other side, the pyrene–porphyrin (PyP) and NIR sensitizers (PyChl and PyBac) [1 mg mL^{-1}] were taken in an ethanol–acetone solution (1 : 1 saturated solution). Furthermore, stock solutions (0.5 mL of each) were mixed and sonicated to completely dissolve the mixture. The resulting mixture (1 mL) was added dropwise in 10 mL of deionized water in RBF *via* a peristaltic pump and then sonicated for 10 min. Then, the

reaction was removed and centrifuged at 10 000 rpm for 8 min for further purification. The final pellet was diluted with deionized water and lyophilized to obtain a dried solid, which was utilized for further analysis.

Determination of the particle size, zeta potential, and morphology of the nanoparticles

The *Z*-average size and surface potential charge of PyP-LNCs, PyChl-LNCs, and PyBac-LNCs were determined using a zeta sizer (Malvern Zetasizer Nano ZS1211332, Malvern, UK). Also, the morphology of these nanoparticles was observed by high-resolution transmission electron microscopy (HR-TEM), whereby a dispersed sample of the nanoparticles (in water) was placed on a copper grid and allowed to air dry. Then, they were observed by TEM microscopy.

Determination of the % loading efficiency of the nanoparticles

The loading efficiency (%) was calculated using a reported protocol and quantified by optical density using UV–vis spectroscopy.[44] After loading the pyrene–porphyrin and NIR sensitizers, the unreacted photosensitizer supernatant was removed and diluted with acetone–ethanol solution. The absorbance was recorded at 418 nm (PyP), 406 nm (PyChl), and 735 nm (PyBac) using UV–vis spectroscopy. The amount of free sensitizer drugs was determined by the standard calibration curves of each sample. The experiment was performed in triplicate for each sample and the results presented as the mean ± standard deviation. The loading efficiency (%) of the nanoformulations was determined by the following equation, and standard curves were also calibrated for the analysis:

$$\text{Loading efficiency \%} = [(\text{Total drug added} - \text{free drug in supernatant})/\text{Total drug added}] \times 100 \quad (4)$$

Spectroscopic analysis

The pyrene–porphyrin (PyP-LNCs), and NIR sensitizers (PyChl-LNCs, and PyBac-LNCs) were analyzed using a UV-Vis spectrophotometer. The analysis was performed in deionized water.

***In vitro* release and stability study of the nanoformulations.** The release of the pyrene–porphyrin and NIR sensitizers pyrene–chlorin and pyrene–bacteriochlorin from pyrene–porphyrin and the NIR sensitizers-loaded lignin nanoparticles (PyP-LNCs, PyChl-LNCs, and PyBac-LNCs) was studied using a previously reported protocol.[20,44] Briefly, 10 mg of each sample of PyP-LNCs, PyChl-LNCs, and PyBac-LNCs was immersed in 10 mL phosphate buffer in two different pH (5 and 7.4) conditions, and then incubated in an orbital incubator shaker at 100 rpm; 37 °C for 24 h. Next, 1 mL aliquots were removed at different time intervals (30 min, and 1, 1.5, 2, 2.5, 3, 3.5, 12, 18, and 24 h.) and replenished with 1 mL volume of phosphate buffer (pH 5 and pH 7.4) to maintain the sink condition. The immersed nanolignin sensitizers were observed for the release of the photosensitizers (**8**, **9a**, and **9b**) into the two different pH buffers (5 and 7.4). The absorbance of each 1 mL aliquot sample of nanolignin sensitizer was measured by the 413 nm (PyP-LNCs), 420 nm (PyChl-LNCs), and 753 nm (PyBac-LNCs) peaks using UV-vis spectroscopy. The standard calibration curves of each photosensitizer (**8**, **9a**, and **9b**) were obtained, and linear regression equations were obtained. Then, the concentration of released photosensitizer was measured using the respective standard calibration equations (Fig. S17, ESI†).

Singlet oxygen quantification of PyP, PyChl, PyBac, and their nanoformulations

Following a reported protocol,[56] the singlet oxygen quantum yield (Φ_Δ) was determined by 1,3-diphenylisobenzofuran (DPBF) dye. Stock solutions of DPBF (1 mg mL^{-1}) were prepared in DMF and DMSO. Furthermore, stock solutions of the photosensitizer molecules [PyP (**8**), PyChl (**9a**), PyBac (**9b**); 1 mg mL^{-1}] and each nanoprobe [(PyP-LNCs, PyChl-LNCs and PyBac-LNCs)] were prepared in DMF and water, respectively. They were then diluted with the respective solvents to maintain a solution with an OD ≤ 1. The DPBF dye (10 μg mL^{-1}) and each photosensitizer molecule (**8**, **9a**, and **9b**) at a 10 μg mL^{-1} concentration, were then irradiated with a green LED light (12 W; 500–570 nm, 32 400 J cm^{-2}) for pyrene–porphyrin (**8**) and red light (12 W; 620–750 nm, 32 400 J cm^{-2}) for the PyChl (**9a**) and PyBac (**9b**) samples. At the same time, the OD for DPBF degradation was recorded at different time intervals (0, 30, 60, 90, 120, 150, and 180 s) at 410 nm. Similarly, the same procedure was followed for the nanoformulations (20 μg mL^{-1}) to record DPBF decay at 417 nm. The SOQY calculations were performed in triplicate for each experiment, and the obtained data were calculated as the mean ± standard deviation using zinc phthalocyanine (ZnPc) as a standard (Φ_Δ, 0.56). The singlet oxygen quantum yield (Φ_Δ) was quantified by the following formula:

$$\Phi_\Delta = \Phi_{\Delta S} \times m_s/m_u \quad (5)$$

where m_u and m_s are the slopes of the unknown and reference, respectively; and $\Phi_{\Delta S}$ is the SOQY value of the reference ZnPc, *i.e.* 0.56.

Microorganisms and culture conditions

The fungal strain *C. albicans* was employed for the study. The fungal cells were grown and incubated in YPD broth (yeast, peptone, and dextrose). The growth of the cells was continued till the OD_{600} reached 0.6.

In vitro ROS generation analysis

The *C. albicans* suspension with an OD_{600} up to 0.6 was reproduced and revived for the analysis. To stain it with dye, 2′,7′-dichlorodihydrofluorescein diacetate (H_2DCFDA) was mixed with the suspension of the *C. albicans* cells and underwent incubation at 100 rpm (at 37 °C) for 30 min. The suspension was removed and centrifuged at 3700 rpm for 5 min. The pellet was removed and washed three times in deionized water. The cells were treated with different doses: 5, 10, and 15 μg mL^{-1} under light (source green/red LED of 12 W) and dark conditions. The fluorescence intensity of each condition

was measured at the excitation wavelength of 485 nm and emission wavelength of 520 nm.

Scanning electron microscopy (SEM) of *C. albicans*. After treatment, the fungal cells were observed using SEM microscopy with all the samples (PyP-LNCs, PyChl-LNCs, and PyBac-LNCs). The fixation of the cells was done using 5% glutaraldehyde in distilled water. Then, images were captured for the control cells and each sample.

DNA-intercalation study

The DNA-intercalation study of the samples was carried out using a DNA plasmid (pUC19) by agarose gel electrophoresis. A 10 μM solution of each sample PyP, PyChl, and PyBac was prepared in DMSO-tris buffer, and 1 mg mL^{-1} of each nanoformulation (PyP-LNCs, PyChl-LNCs, and PyBac-LNCs) was prepared in distilled water. Before the electrophoresis, they were incubated at 37 °C for 1 h. Next, 0.25 μg of DNA plasmid pUC19 was taken, mixed with each sample, and incubated at 37 °C for 1 h, and the total reaction volume was 14 μL. The agarose gel-electrophoresis of PyP (**8**), PyChl (**9a**), PyBac (**9b**) and each nanoprobe (PyP-LNCs, PyChl-LNCs, and PyBac-LNCs) (tris buffer, 1 h) was done to prove the ability to intercalate the DNA.

EtBr and DAPI displacement study

For the displacement of DAPI/EtBr, 2.5 μg DNA in 500 μL molecular biology grade water containing EtBr/DAPI was incubated for 1 h. After the incubation, 100 μM PyP/PyChl/PyBac was added and incubated to displace the DAPI/EtBr. The fluorescence intensities were recorded from 400 to 800 nm with excitation at 480 and 358 nm wavelength for DAPI and EtBr, respectively.

Fluorescence imaging

The *C. albicans* cells were incubated with 20 μg mL^{-1} of each nanoprobe PyP-LNCs, PyChl-LNCs, and PyBac-LNCs at 37 °C for 1 h. They were washed in distilled water, pelleted, and resuspended in 50 μL distilled water and chemically fixed using 5% glutaraldehyde in distilled water. Also, the fluorescence imaging was validated by staining the *Candida* cells with 20 μg mL^{-1} of 4′,6-diamidino-2-phenyl-indole (DAPI, blue fluorescent stain) in distilled water. They were also washed in distilled water, pelleted, and resuspended in 50 μL distilled water and chemically fixed using 5% glutaraldehyde in distilled water. Next, 10 μL of each sample was placed on a microscope slide and covered with a coverslip. Then, they were observed by a fluorescence microscope (Nikon; TS2FL) with a 2880 × 2048 pixel resolution. An excitation wavelength of 525 nm was used to capture the dark field images and a 650 to 755 nm bandpass filter for the red-light absorbing pyrene–chlorin and near-IR pyrene–bacteriochlorin.

In vitro photoinactivation study of *Candida albicans* by PyP, PyChl, PyBac, and their nanoformulations

The *Candida albicans* were aerobically grown in YPD broth (yeast, peptone, and dextrose) for 12 h at 37 °C and 100 rpm in an orbital shaking incubator. The broth was then centrifuged and washed three times with deionized water. The OD_{600} of the broth was maintained at 0.6, corresponding to *ca.* 10^3 CFU per mL. Then, 1 mL diluted suspension of the *C. albicans* cells was taken and treated with the synthesized photosensitizers (PyP, PyChl, and PyBac), and the developed nanolignin sensitizers (PyP-LNCs, PyChl-LNCs, and PyBac-LNCs). The common dose concentrations were 0, 5, 10, 15, 20, and 25 μg mL^{-1} for all the samples. These concentrations of pyrene–porphyrin (PyP) and their nanolignin sensitizers (PyP-LNCs) were individually incubated with *C. albicans* for 45 min and further irradiated for about 40 min with a green LED (12 W; 500–570 nm, 32 400 J cm^{-2}) light. Whereas, pyrene–chlorin (PyChl), pyrene–bacteriochlorin (PyBac), and their nanolignin sensitizers (PyChl-LNCs, and PyBac-LNCs) were incubated with *C. albicans* for 45 min and irradiated for about 40 min with a red LED (12 W; 620–750 nm, 32 400 J cm^{-2}) light. After each treatment, 100 μL suspension was withdrawn and plated on the YPD Agar culture plates. Then, they were incubated at 37 °C and examined after 24 h. The grown colonies were counted, and the colony-forming unit (CFU) method was used to determine the % cell viability after each set of treatments. The IC_{50} value of all the samples was determined using a standard linear calibration equation drawn at 0, 5, 10, 15, 20, and 25 μg mL^{-1} doses of PyP, PyChl, PyBac, and nanolignin sensitizers (PyP-LNCs, PyChl-LNCs, and PyBac-LNCs).

Conclusion

In summary, we developed pyrene-substituted NIR photosensitizers, namely chlorin and bacteriochlorin, from their respective porphyrin derivatives. TD-DFT calculations with these NIR fluorescence imaging agents were performed to correlate the experimental photophysical properties with the *in silico* optical studies results. Owing to their hydrophobicity, the NIR photosensitizers were loaded in lignin nanoparticles to form hydrophilic nanolignin sensitizers, which facilitated fluorescence imaging. Due to the presence of pyrene fluorophores, the native near-IR photosensitizers and their corresponding nanoformulations displayed higher DNA binding affinities and enhanced fluorescence properties than porphyrin. Furthermore, the nanolignin sensitizers were found to be promising ROS generators. Conclusively, it was demonstrated that the pyrene-based near-IR photosensitizers (chlorin and bacteriochlorin) are promising candidates for red and near-IR light-assisted photodynamic therapy and bioimaging applications.

Data availability

All data supporting the findings of this study are available within the paper and its ESI.†

Conflicts of interest

There are no conflicts to declare.

Acknowledgements

JB thanks the Department of Biotechnology (DBT), Govt. of India for funding the lignin valorization flagship project. K. G. acknowledges CIAB for a senior research fellowship and University Institute of Pharmaceutical Sciences, Panjab University, for PhD registration. S. K. acknowledges the Women Scientists Scheme A (WOS-A), DST, and Govt. of India. A. K. P. thanks CIAB for a senior research fellowship and IISER Mohali for PhD registration. D. M. thanks DBT for a junior research fellowship and IISER Mohali for PhD registration. The authors want to acknowledge the Center of Innovative and Bioprocessing (CIAB), Department of Biotechnology (DBT), Govt. of India for funding and infrastructural support.

References

1 Y. Zhang, P. Huang, D. Wang, J. Chen, W. Liu, P. Hu, M. Huang, X. Chen and Z. Chen, *Nanoscale*, 2018, **10**, 15485–15495.
2 L. Huang, Y. Y. Huang, P. Mroz, G. P. Tegos, T. Zhiyentayev, S. K. Sharma, Z. Lu, T. Balasubramanian, M. Krayer, C. Ruzié, E. Yang, H. L. Kee, C. Kirmaier, J. R. Diers, D. F. Bocian, D. Holten, J. S. Lindsey and M. R. Hamblin, *Antimicrob. Agents Chemother.*, 2010, **54**, 3834–3841.
3 D. M. George, A. S. Vincent and H. R. Mackey, *Biotechnol. Rep.*, 2020, **28**, e00563.
4 M. K. Peters, F. Röhricht, C. Näther and R. Herges, *Org. Lett.*, 2018, **20**, 7879–7883.
5 W. Zhu, Y. H. Gao, P. Y. Liao, D. Y. Chen, N. N. Sun, P. A. Nguyen Thi, Y. J. Yan, X. F. Wu and Z. L. Chen, *Eur. J. Med. Chem.*, 2018, **160**, 146–156.
6 Z. Yu and M. Ptaszek, *Org. Lett.*, 2012, **14**, 3708–3711.
7 X.-D. Jiang, D. Xi, C.-L. Sun, J. Guan, M. He and L.-J. Xiao, *Tetrahedron Lett.*, 2015, **56**, 4868–4870.
8 H. S. Lee, J. H. Han, J. H. Park, M. E. Heo, K. Hirakawa, S. K. Kim and D. W. Cho, *Phys. Chem. Chem. Phys.*, 2017, **19**, 27123–27131.
9 P. A. Panchenko, M. A. Grin, O. A. Fedorova, M. A. Zakharko, D. A. Pritmov, A. F. Mironov, A. N. Arkhipova, Y. V. Fedorov, G. Jonusauskas, R. I. Yakubovskaya, N. B. Morozova, A. A. Ignatova and A. V. Feofanov, *Phys. Chem. Chem. Phys.*, 2017, **19**, 30195–30206.
10 J. H. Han, H. Y. Cho, D. Y. Kim, Y. J. Jang, Y.-A. Lee and S. K. Kim, *J. Mol. Struct.*, 2020, **1215**, 128264.
11 N. A. Le, V. Babu, M. Kalt, L. Schneider, F. Schumer and B. Spingler, *J. Med. Chem.*, 2021, **64**, 6792–6801.
12 M. Wu, Z. Liu and W. Zhang, *Chem. Sci.*, 2021, **12**, 1295–1301.
13 L. Huang, M. Krayer, J. G. S. Roubil, Y. Y. Huang, D. Holten, J. S. Lindsey and M. R. Hamblin, *J. Photochem. Photobiol., B*, 2014, **141**, 119–127.
14 B. Pucelik, A. Sułek and J. M. Dąbrowski, *Coord. Chem. Rev.*, 2020, **416**, 213340.
15 X. Zhang, Y. Ma, X. Zhang, X. Pang and Z. Yang, *Biomed. Pharmacother.*, 2023, **165**, 115014.
16 N. Dragicevic, J. Predic-Atkinson, B. Nikolic, S. B. Pajovic, S. Ivkovic and M. Adzic, *Expert Opin. Drug Delivery*, 2024, **21**, 279–307.
17 V. M. Desai, M. Choudhary, R. Chowdhury and G. Singhvi, *Mol. Pharmacol.*, 2024, **21**, 1591–1608.
18 M. Tavakkoli Yaraki, B. Liu and Y. N. Tan, *Nano-Micro Lett.*, 2022, **14**, 1–49.
19 G. Li, R. Zhou, W. Zhao, B. Yu, J. Zhou, S. Liu, W. Huang and Q. Zhao, *Research*, 2020, **2020**, 1–14.
20 S. Paul, A. De, S. Kirar, N. S. Thakur, A. K. Pujari, K. Gogde and J. Bhaumik, *ACS Appl. Nano Mater.*, 2024, **7**(9), 10984–10997.
21 S. Paul, N. S. Thakur, S. Chandna, Y. N. Reddy and J. Bhaumik, *J. Mater. Chem. B*, 2021, **9**, 1592–1603.
22 A. K. Pujari, R. Kaur, Y. N. Reddy, S. Paul, K. Gogde and J. Bhaumik, *J. Med. Chem.*, 2024, **67**, 2004–2018.
23 J. H. Lee, K. Kim, X. Jin, T. M. Kim, I. G. Choi and J. W. Choi, *Int. J. Biol. Macromol.*, 2021, **183**, 660–667.
24 R. Kumar, A. Butreddy, N. Kommineni, P. Guruprasad Reddy, N. Bunekar, C. Sarkar, S. Dutt, V. K. Mishra, K. R. Aadil, Y. K. Mishra, D. Oupicky and A. Kaushik, *Int. J. Nanomed.*, 2021, **16**, 2419–2441.
25 D. A. Ali and M. M. Mehanna, *Int. J. Biol. Macromol.*, 2022, **221**, 934–953.
26 J. H. Lee, J. S. Im, X. Jin, T. M. Kim and J. W. Choi, *ACS Sustainable Chem. Eng.*, 2022, **10**, 5792–5802.
27 M. Mishra, *Lignin-based Materials*, 2023, pp. 223–246.
28 M. Arcentales, R. Martín-Sampedro, R. Santos-Oliveira, M. F. Attia, J. N. Anker, D. C. Whitehead, A. Debut, L. Deng, Y. Zheng, B. Hu, M. P. Romero, F. López and F. Alexis, *ACS Appl. Mater. Interfaces*, 2023, **15**, 31320–31329.
29 A. Boarino, H. Wang, F. Olgiati, F. Artusio, M. Özkan, S. Bertella, N. Razza, V. Cagno, J. S. Luterbacher, H. A. Klok and F. Stellacci, *ACS Sustainable Chem. Eng.*, 2022, **10**, 14001–14010.
30 B. F. O. Nascimento, A. M. d A. Rocha Gonsalves and M. Pineiro, *Inorg. Chem. Commun.*, 2010, **13**, 395–398.
31 H. W. Whitlock, R. Hanauer, M. Y. Oester and B. K. Bower, *J. Am. Chem. Soc.*, 1969, **91**, 7485–7489.
32 J. Bhaumik, Z. Yao, K. E. Borbas, M. Taniguchi and J. S. Lindsey, *J. Org. Chem.*, 2006, **71**, 8807–8817.
33 J. K. Laha, S. Dhanalekshmi, M. Taniguchi, A. Ambroise and J. S. Lindsey, *Org. Process Res. Dev.*, 2003, **7**, 799–812.
34 R. Paolesse, A. Marini, S. Nardis, A. Froiioa, F. Mandoj, D. J. Nurco, L. Prodi, M. Montalti and K. M. Smith, *J. Porphyrins Phthalocyanines*, 2012, **7**, 25–36.
35 J. Bhaumik, N. S. Thakur, P. K. Aili, A. Ghanghoriya, A. K. Mittal and U. C. Banerjee, *ACS Biomater. Sci. Eng.*, 2015, **1**, 382–392.
36 K. Gogde, S. Paul, A. K. Pujari, A. K. Yadav and J. Bhaumik, *J. Med. Chem.*, 2023, **66**, 13058–13071.
37 M. J. Frisch, G. W. Trucks, H. B. Schlegel, G. E. Scuseria, M. A. Robb, J. R. Cheeseman, G. Scalmani, V. Barone, G. A. Petersson, H. Nakatsuji, X. Li, M. Caricato, A. V. Marenich, J. Bloino, B. G. Janesko, R. Gomperts, B. Mennucci, H. P. Hratchian, J. V. Ortiz, A. F. Izmaylov,

J. L. Sonnenberg, D. Williams-Young, F. Ding, F. Lipparini, F. Egidi, J. Goings, B. Peng, A. Petrone, T. Henderson, D. Ranasinghe, V. G. Zakrzewski, J. Gao, N. Rega, G. Zheng, W. Liang, M. Hada, M. Ehara, K. Toyota, R. Fukuda, J. Hasegawa, M. Ishida, T. Nakajima, Y. Honda, O. Kitao, H. Nakai, T. Vreven, K. Throssell, J. A. Montgomery, J. E. Peralta, F. Ogliaro, M. J. Bearpark, J. J. Heyd, E. N. Brothers, K. N. Kudin, V. N. Staroverov, T. A. Keith, R. Kobayashi, J. Normand, K. Raghavachari, A. P. Rendell, J. C. Burant, S. S. Iyengar, J. Tomasi, M. Cossi, J. M. Millam, M. Klene, C. Adamo, R. Cammi, J. W. Ochterski, R. L. Martin, K. Morokuma, O. Farkas, J. B. Foresman and D. J. Fox, *Gaussian 16, C.01*, 2016.

38 M. Gouterman, *J. Mol. Spectrosc.*, 1961, **6**, 138–163.

39 O. Cramariuc, T. I. Hukka and T. T. Rantala, *J. Phys. Chem. A*, 2004, **108**, 9435–9441.

40 Z. Melissari, H. C. Sample, B. Twamley, R. M. Williams and M. O. Senge, *ChemPhotoChem*, 2020, **4**, 601–611.

41 S. K. Sharma, M. Krayer, F. F. Sperandio, L. Huang, Y. Y. Huang, D. Holten, J. S. Lindsey and M. R. Hamblin, *J. Porphyrins Phthalocyanines*, 2013, **17**, 73–85.

42 Y. N. Reddy, K. Gogde, S. Paul and J. Bhaumik, in *Biomass for Bioenergy and Biomaterials*, ed. N. Adlakha, R. Bhatnagar and S. S. Yazdani, CRC Press, Boca Raton, Florida, 2021, pp. 31–64.

43 D. Yang, S. Gao, Y. Fang, X. Lin, X. Jin, X. Wang, L. Ke and K. Shi, *Nanomedicine*, 2018, **13**, 3159–3177.

44 A. Shalviri, G. Raval, P. Prasad, C. Chan, Q. Liu, H. Heerklotz, A. M. Rauth and X. Y. Wu, *Eur. J. Pharm. Biopharm.*, 2012, **82**, 587–597.

45 P. Carloni, E. Damiani, L. Greci, P. Stipa, F. Tanfani, E. Tartaglini and M. Wozniak, *Res. Chem. Intermed.*, 1993, **19**, 395–405.

46 S. Kirar, N. S. Thakur, J. K. Laha and U. C. Banerjee, *ACS Appl. Bio Mater.*, 2019, **2**, 4202–4212.

47 M. Haeubl, L. M. Reith, B. Gruber, U. Karner, N. Müller, G. Knör and W. Schoefberger, *J. Biol. Inorg. Chem.*, 2009, **14**, 1037–1052.

48 B. P. de Oliveira, N. U. de, C. Bessa, J. F. do Nascimento, C. S. de Paula Cavalcante, R. O. dos, S. Fontenelle and F. O. M. da S. Abreu, *Int. J. Biol. Macromol.*, 2023, **227**, 805–814.

49 J. Pfister, A. Lichius, D. Summer, H. Haas, T. Kanagasundaram, K. Kopka and C. Decristoforo, *Sci. Rep.*, 2020, **10**, 1–9.

50 M. Bera, M. Das, M. Dolai, S. Laha, M. M. Islam, B. C. Samanta, A. Das, I. Choudhuri, N. Bhattacharyya and T. Maity, *ACS Omega*, 2023, **8**, 636–647.

51 M. Das, S. Mukherjee, M. M. Islam, I. Choudhuri, N. Bhattacharyya, B. C. Samanta, B. Dutta and T. Maity, *ACS Omega*, 2022, **7**, 23276–23288.

52 E. M. Kojic and R. O. Darouiche, *Clin. Microbiol. Rev.*, 2004, **17**, 255.

53 M. Nitz, B. W. Purse and D. R. Bundle, *Org. Lett.*, 2000, **2**, 2939–2942.

54 K. M. Sakita, P. C. V. Conrado, D. R. Faria, G. S. Arita, I. R. G. Capoci, F. A. V. Rodrigues-Vendramini, N. Pieralisi, G. B. Cesar, R. S. Gonçalves, W. Caetano, N. Hioka, E. S. Kioshima, T. I. E. Svidzinski and P. S. Bonfim-Mendonça, *Future Microbiol.*, 2019, **14**, 519–531.

55 N. Martins and C. F. Rodrigues, *J. Clin. Med*, 2020, **9**, 722.

56 Y. N. Reddy, N. Singh Thakur and J. Bhaumik, *ChemNanoMat*, 2020, **6**, 239–247.

